The complement system supports normal postnatal development and gonadal function in both sexes

Authors:
Arthur S. Lee[1], Jannette Rusch[1], Abul Usmani[1], Ana C. Lima[1], Wendy S.W. Wong[2], Ni Huang[1], Maarja Lepamets[3], Katinka A. Vigh-Conrad[4], Ronald E. Worthington[5], Reedik Mägi[3], John E. Niederhuber[2,6], Xiaobo Wu[7], John P. Atkinson[7], Rex A. Hess[8], Donald F. Conrad[1,5*]

Affiliations:
[1] Department of Genetics, Washington University School of Medicine, St. Louis, Missouri, USA
[2] Inova Translational Medicine Institute (ITMI), Inova Health Systems, Falls Church, Virginia, USA.
[3]Estonian Genome Center, University of Tartu, Tartu, Estonia
[4]Department of Pathology and Immunology, Washington University School of Medicine, St. Louis, Missouri, USA
[5] Department of Pharmaceutical Sciences, University of Southern Illinois, Edwardsville, Illinois, USA
[6]Johns Hopkins University School of Medicine, 733 North Broadway Street, Baltimore, MD, USA
[7]Division of Rheumatology, Department of Medicine, Washington University School of Medicine, St. Louis, Missouri, USA
[8] College of Veterinary Medicine, University of Illinois, Urbana-Champaign, Illinois, USA

***Corresponding Author:**

Dr. Donald F. Conrad
Department of Genetics
Washington University School of Medicine
Campus Box 8232
St. Louis MO, 63110, USA
E-mail: don.conrad@wustl.edu

Abstract: Male and female infertility are clinically managed and classified as distinct diseases, and relatively little is known about mechanisms of gonadal function common to both sexes. We used genome-wide genetic analysis on 74,896 women and men to find rare genetic variants that modulate gonadal function in both sexes. This uncovered an association with variants disrupting *CSMD1*, a complement regulatory protein located on 8p23, in a genomic region with an exceptional evolution. We found that *Csmd1* knockout mice display a diverse array of

gonadal defects in both sexes, and in females, impaired mammary gland development that leads to increased offspring mortality. The complement pathway is significantly disrupted in *Csmd1* mice, and further disruption of the complement pathway from joint inactivation of *C3* leads to more extreme reproductive defects. Our results can explain a novel human genetic association with infertility and implicate the complement system in the normal development of postnatal tissues.

Keywords: GWAS, fertility, primary ovarian insufficiency, azoospermia, complement

Introduction

Male and female infertility have historically been classified and clinically treated as distinct disease entities and this perspective has led to the assembly of many cohorts for the study of sex-specific reproductive processes (Hotaling and Carrell, 2014; Nelson, 2009; O'Flynn O'Brien et al., 2010; Stolk et al., 2012). However, many molecular and physiological mechanisms of fertility regulation are shared between male and female mammals including embryonic gonad development, meiosis, and the hypothalamic-pituitary-gonadal axis (Matzuk and Lamb, 2008). There are other phenomena common to gonadal function in both sexes that are poorly understood, and the extent to which these phenomena have a common set of regulators is unknown. For instance, programmed germ cell degeneration is a pervasive part of gonadal biology in both sexes. In human males, roughly 80% of the meiotic descendants of spermatogonial stem cells undergo apoptosis prior to ever becoming spermatozoa (Hess and Renato de Franca, 2008). In human females, nearly 80% of the oocytes made during embryogenesis are eliminated by birth, representing the first major stage of oocyte loss (Baker, 1963; Kurilo, 1981). Upon menarche, a woman will ovulate approximately 400 times in her life.

63 However, of 300,000-500,000 oocytes present at birth, only roughly 1,000 survive the sojourn to
64 menopause, representing colossal germ cell loss not attributable to ovulation (Wallace and
65 Kelsey, 2010). The mean ratio of surviving : apoptotic germ cells differs between species, but is
66 narrowly regulated within species (Hsueh et al., 1994) (Hess and Renato de Franca, 2008). Germ
67 cell loss in both sexes may represent a cellular safeguard against violation of essential cellular
68 events such as DNA replication/repair and chromosome segregation--events that occur prior to,
69 or during, meiosis. Spermiogenesis and folliculogenesis, which occur after the onset of meiosis,
70 are highly complex in their own right. Molecular mechanisms for error-checking these processes
71 are poorly understood.
72 Defects in the development of germ cells that are due to problems originating in the gonad are
73 clinically defined as primary gonadal dysfunction. Primary gonadal dysfunction is an infertility
74 phenotype that is attractive for human genetic analysis, has a prevalence of at least 1% in males
75 and females (Luborsky et al., 2003; Willott, 1982), and has clear diagnostic criteria. In males,
76 primary gonadal dysfunction can manifest as a total absence of germ cells, an arrest of
77 spermatogenesis, or complete but limited sperm production. In females the presentation can
78 range from complete absence of germ cells to irregular ovulation or premature menopause.
79 We have previously identified a reproducible association between rare copy number variant
80 (CNV) burden and male gonadal dysfunction (Huang et al., 2015; Lopes et al., 2013). In the present
81 study, we used array and exome sequencing data from a large cohort of post-menopausal women,
82 collected as part of the Women's Health Initiative study (Chen et al., 2012), to identify novel,
83 shared factors required for normal gonadal function in both sexes, and replicated our findings
84 with data from the UK Biobank(Sudlow et al., 2015).

85

86 ## RESULTS

87 ### Rare *CSMD1* mutations are associated with reproductive outcomes in humans

88 Due to the strong selective pressure against infertility mutations, we hypothesized that male and
89 female gonadal dysfunction are driven largely by rare mutation events. To test this hypothesis,
90 we acquired SNP array and phenotype data from 12,002 women (515 cases of inferred primary
91 ovarian insufficiency (POI) vs. 11,487 normal menopause controls) and 2,072 men (321 cases of
92 spermatogenic impairment vs. 1,751 controls) with known reproductive health history. Since it is
93 difficult to detect rare variants via conventional SNP arrays, we leveraged the SNP log R ratios
94 and B-allele frequencies to discover CNVs that occupy the entire allele frequency spectrum
95 (**Table S1, Methods**). We then applied filters to enrich for deleterious CNVs (minor allele
96 frequency < 0.01 and length > 100 kb). We used these CNVs to perform a rare variant, gene-
97 based, case-control genome wide association study (GWAS) separately in males and females
98 (**Methods**).

99 Our rare variant GWAS identified a significant association between inferred POI and deletions
100 overlapping the CUB and Sushi multiple domains 1 (*CSMD1*) gene located on chromosome
101 8p23.2 (OR = 16; nominal p-value=4.0 x 10^{-4}; genome-wide p-value= 0.015; **Figure 1A**). This
102 association signal replicated in our smaller cohort of male spermatogenic impairment (OR = 3.3;
103 nominal p-value = 6.5 x 10^{-3}). This CNV association is largely driven by the observation of an
104 aggregate enrichment of rare deletions in cases, compared to controls, all of which are clustered
105 in the 5' half of the gene, in introns 1-3 (**Figures 1B)** There was no single CNV in the region
106 with a significant frequency difference between cases and controls.

107 To replicate the association between deletions in *CSMD1* and risk for gonadal dysfunction, we
108 constructed another POI case-control cohort using the UK Biobank (**Methods**). After CNV QC
109 and rigorous case/control selection, we obtained a cohort of 63,064 women with both reliable
110 phenotype data and CNV calls; 1,873 of these were considered cases of POI. We again observed
111 a significant association between POI and rare deletions in introns 1-3 of *CSMD1* (0.6%
112 frequency in cases, 0.2% in controls, OR=3.03, $p < 5 \times 10^{-4}$, Figure 1A and 1B). To succinctly
113 summarize the risk conferred by rare (<1% MAF) deletions in introns 1-3 of *CSMD1*, we
114 performed a meta-analysis across all three cohorts, this time considering deletions of all sizes,
115 and found a frequency of 0.7% in cases and 0.2% in controls (meta-analysis $p = 4.8 \times 10^{-5}$;
116 **Figure 1C**). The list of deletions observed in introns 1-3 are provided as **Table S2**.
117
118 To further replicate our findings using an orthogonal genotyping platform, we analyzed single
119 nucleotide variants (SNVs) ascertained by whole-exome sequencing generated from the female
120 cohort (n = 1,526). Employing SKAT, a gene-based quantitative trait association framework, we
121 identified a significant association between rare (MAF < 0.01), deleterious *CSMD1* single
122 nucleotide variants and age at menopause (p-value $< 5 \times 10^{-3}$; **Methods**). The bulk (97.1%) of
123 the *CSMD1* protein product consists of alternating CUB (**c**omplement C1r/C1s, **U**egf, **B**mp1) and
124 Sushi/CCP (**c**omplement **c**ontrol **p**rotein) domains. We used linear models to further partition the
125 association signal among these two domains. The *CSMD1* SNV association was driven almost
126 exclusively by rare, deleterious mutations in the CUB ($\beta_{CUB} = -0.86$), but not Sushi ($\beta_{SUSHI} =$
127 0.046) domains (P = 0.043; for difference in effect size; **Figure 1D**). We estimate that each rare,
128 deleterious mutation that we detected in CUB domains of *CSMD1* accelerates the onset of
129 menopause by 10 months. These results immediately cast light on the relative importance of the

130 CUB domain in the etiology of infertility, and prioritizes a potential target domain for therapy.
131 Finally, while this work was in progress, a well-powered common variant GWAS in a female
132 cohort of 182,416 individuals identified 3 common SNPs over *CSMD1* to be significantly and
133 independently associated with age at menarche: rs2688325 ($p=2.1 \times 10^{-9}$), rs7828501 ($p=1.2 \times$
134 10^{-13}), and rs7463166 ($p=1.3 \times 10^{-8}$) (Perry et al., 2014). These 3 associations were replicated in
135 ~300,000 individuals: rs2688326 ($p = 4.34 \times 10^{-18}$), rs2724961 ($p = 3.76 \times 10^{-33}$), and rs4875424
136 ($p = 1.99 \times 10^{-16}$) (Day et al., 2017). Remarkably, these 3 common variant associations co-
137 localize to the same 1Mb window as the rare disease-associated deletions described above
138 (**Figure 1B**). Subsequent work has shown that age at menarche and menopause are positively
139 correlated and that the common variants in *CSMD1* associated with age at menarche correctly
140 predicted age at menopause in the expected direction ($\beta_{rs2688325} = 0.014 +/- 0.023$; $\beta_{rs7828501} =$
141 $0.021 +/- 0.020$; $\beta_{rs7463166} = 0.031 +/- 0.021$) (Day et al., 2015). In summary, we detected
142 associations between rare variants in *CSMD1* and gonadal dysfunction i) across multiple classes
143 of genetic variation; ii) ascertained by orthogonal genotyping platforms; iii) occupying multiple
144 points along the allele frequency spectrum; and iv) in multiple populations and cohorts.

145 **The d*e novo* mutation rate across *CSMD1* is exceptionally high in humans**

146 Excluding the Y chromosome, the distal arm of chromosome 8p contains the region of the
147 genome with the greatest intra-population nucleotide diversity and the greatest nucleotide
148 divergence between human and chimpanzee (Nusbaum et al., 2006). This signal of diversity and
149 divergence peaks over *CSMD1* in a 1 Mb region that was originally reported to have an average
150 human-chimpanzee divergence of 0.032 substitutions/bp, or 8.6 s.d. above the genomic mean.
151 Multiple, non-exclusive factors can influence nucleotide diversity at a locus, namely mutation
152 rate, demographic history, and natural selection. To evaluate the effect (if any) of mutation rate

153 separate from confounding factors such as demography and long-term selection, we measured
154 directly the number of *de novo* mutations (DNMs) across chromosome 8 in 709 human parent-
155 offspring trios, calculating the average mutation rate in non-overlapping 100kb windows
156 (**Methods**). We observed a local enrichment of DNMs overlapping *CSMD1*, as the mutation rate
157 in six of the twenty 100kb windows over the gene was estimated to be greater than 6 x 10^{-8}
158 mutations/bp/generation, a five-fold increase above the genomic average of 1.2 x 10^{-8} (**Figure**
159 **1E)**. The "hottest" mutation hotspot we observed in the region had a DNM rate of 1.48 x 10^{-7}, at
160 3.9 Mb-4.0 Mb, located within the nexus of infertility risk mutations reported above. This
161 enrichment of DNMs is not well-explained by the intrinsic mutability of the primary nucleotide
162 sequence in this region (**Figure 1E; Methods**). Using an association study on the same cohort of
163 trios, we tested the region for *cis*-acting variants that might predispose to genome instability and,
164 as an indirect result, infertility, but were unable to find a replicable association (data not shown).
165

166 **CSMD1 is expressed at the interface of germ cells and somatic cells in male and female**
167 **gonads**

168
169 *CSMD1* encodes for an extremely large (>3,000 amino acid) transmembrane protein with a large
170 extracellular portion consisting of alternating CUB and Sushi complement-interacting domains
171 (Kraus et al., 2006). The protein encoded by *CSMD1* is conserved between human and mouse,
172 with 93% amino acid identity and 100% identity of the number and ordering of CUB and Sushi
173 domains (**Figure 2A**). *CSMD1* and its mammalian orthologs are expressed in both male and
174 female gonads, but little is known of its molecular function, particularly in the context of
175 fertility. To elucidate CSMD1's function, we first performed RNA-seq on whole mouse testes
176 and ovaries. *Csmd1* is expressed in both tissues (**Figure 2B**), consistent with previous work

177 (Soumillon et al., 2013; Steen et al., 2013)**.** In testes, *Csmd1* is minimally expressed at 20 days
178 and more robustly expressed at 40 days of age which coincides with the onset of sexual maturity.
179 Mammalian testes demonstrate exceptional transcriptional complexity in comparison to other
180 tissues, owing to the highly coordinated spatial and temporal synchronization required for proper
181 spermatogenesis (Soumillon et al., 2013). Therefore, to capture a detailed transcriptional profile
182 of *Csmd1*, we purified individual germ cell types using FACS (**Figure S1A**). Subsequent RNA-
183 seq of purified germ cells reveals low levels of *Csmd1* expression during the diploid cell stages
184 (i.e., spermatogonia and primary spermatocytes), and peak expression at the haploid stages (i.e.,
185 secondary spermatocytes and spermatids) (**Figure 2B**; **Figure S1B**). Finally, *in situ* antibody
186 immunofluorescence on testis cross sections using a validated antibody (**Figure S2**)
187 demonstrates that CSMD1 protein is expressed at the cell membrane at multiple stages of
188 spermatogenesis, including at the interface of elongated spermatids and Sertoli cells, but is
189 absent from spermatozoa, consistent with mRNA expression data (**Figure 2C**; **Figure S1C**). We
190 performed immunofluorescence (IF) staining for key markers on whole-mount longitudinal
191 preparations of individual seminiferous tubules to examine the interface between germ cells,
192 Sertoli cells, and cells in the interstitial space. CSMD1 is expressed in a hatched pattern which is
193 reminiscent of the actin bundles found at the Sertoli-Sertoli blood testis barrier and the Sertoli-
194 spermatid interface (**Figure 2D**) (Lie et al., 2010).
195 Detailed analysis of the distribution of CSMD1 protein within the ovary revealed parallels with
196 the testis. As in the testes, CSMD1 shows lower expression in follicles bearing diploid germ cells
197 (i.e., primordial and primary follicles) and higher expression in follicles bearing haploid germ
198 cells (i.e., secondary, tertiary, and pre-ovulatory follicles; **Figure 2E**). Theca cells also stain
199 positive, as is quite apparent on late stage follicles (**Figure 2E**). The post-ovulatory corpus

200 luteum shows no specific CSMD1 expression (dotted lines; **Figure 2F**). As with male germ cells,
201 female oocytes require substantial physical interaction with surrounding somatic cells (Li and
202 Albertini, 2013). At high magnification, CSMD1 is expressed along transzonal projections that
203 emanate from the granulosa cells and connect to the oocyte membrane (**Figure 2F**).
204

205 ## *Csmd1* knockout disrupts postnatal cellular development in multiple male and female
206 tissues in mice

207

208 To confirm the biological role of *CSMD1* in male and/or female gonadal function, we perturbed
209 its ortholog in a model organism. We generated a colony of *Csmd1* wildtype, heterozygous, and
210 knockout mice and observed the effect of genotype on gonadal function and fertility (**Methods,**
211 **Figure 3D**). In males, gross testis weight at necropsy did not differ significantly among
212 wildtype, heterozygote, and knockout mice when measured in aggregate ($P = 0.69$). However, a
213 subset of *Csmd1* knockout males suffer from profound anatomical and histological derangement
214 of the testes (**Figure 3**; **Figure S3**). Remarkably, the most extreme instances of testes
215 degeneration, Sertoli cell-only tubules, could be observed as early as 34 days of age (**Figure 3A**;
216 **Figure S3B**). This time point corresponds to the onset of male sexual maturity (approximately
217 30-40 days) and the emergence of the spermatid germ cell stage, where *Csmd1* is maximally
218 expressed. Males showed no evidence of derangement prior to sexual maturity (**Figure S3C**).
219 Severity ("none", "mild", and "profound") and onset (postnatal day 34 through day 300) of the
220 degeneration phenotype vary greatly between individuals. In fact, different foci within the same
221 testis of *Csmd1* knockout mice often show different stages of degeneration (**Figure 3B**). Our
222 histological study of over 50 knockout animals uncovered two types of germ cell pathology

223 whose connection to each other is unclear. The first is a sequence of active loss of germ cells
224 within each tubule (**Figure 3B**). Spermatogenesis begins to become disorganized, especially at
225 the late stages of spermiogenesis, with failure of spermiation, fewer numbers of elongating
226 spermatids in the lumen, and mixing of spermatid steps in stages IX-XII. This is followed by the
227 sloughing of all types of germ cells into the lumen; remaining germ cells can be observed in
228 unusual tubules that appear to be missing one or more waves of spermatogenesis, and these
229 eventually resolve as Sertoli cell-only tubules. Sloughed germ cells can be seen downstream in
230 the epididymis, and, occasionally they obstruct the rete testis leading to dilation of the tubules
231 (data not shown). These defects are most likely to arise due to disruption of interactions between
232 Sertoli and germ cells. The second pathology was an apparent depletion of spermatogonial stem
233 cells in the atrophic tubules; even in tubules with ongoing spermatogenesis, some areas show no
234 spermatogonia. Significantly fewer germ cells express the male germ cell antigen TRA98+
235 (Poisson regression; $P < 2 \times 10^{-16}$; **Figures 3D and S3D**), in both atrophic and normal tubules,
236 suggesting that knockout testes suffer from expression perturbations in addition to, or perhaps
237 presaging, loss of spermatogonia and frank degeneration. Together, these observations indicate
238 that the *Csmd1* knockout mutation (i) is not fully penetrant; and (ii) may be influenced by
239 environmental and/or stochastic events. However, even after accounting for age covariates,
240 *Csmd1* genotype segregates significantly with testes derangement status ($P = 7.69 \times 10^{-3}$;
241 MANOVA; **Figure 3C**). Finally, we performed serial backcrossing for 9 generations on a subset
242 of mice to validate the effect of the *Csmd1* null allele on a roughly constant genetic background
243 (**Methods**). We recapitulated the degeneration phenotype in these backcrossed male knockouts
244 (**Figure S3E**), indicating that *Csmd1* genotype status—not genetic background—was driving this
245 signal of degeneration.

246 In females, we observed severe inflammatory changes associated with foam cell infiltration, and,
247 rarely, ovarian cysts in a subset of *Csmd1* knockouts (**Figures 4A and 4B**). Foam cells are
248 multinucleated phagocytic macrophages which have become engorged with lipid, and are
249 associated with ovarian aging. We performed Oil Red O staining which showed highly elevated
250 lipid signal in the ovarian stroma of knockouts compared to age-matched controls, indicating a
251 phenotype of premature ovarian aging in knockout animals (**Figure 4A**). *Csmd1*-deficient
252 females had significantly smaller ovaries by mass when controlling for age, ($p = 8.1 \times 10^{-3}$;
253 **Figure 3D; Figure 4C**). Furthermore, knockout females showed significantly more atretic
254 follicles and fewer normal pre-ovulatory follicles at necropsy ($p=3.5 \times 10^{-3}$; Hotelling t-test;
255 **Figure 4D**). To evaluate whether these biometric and histologic changes were also associated
256 with reproductive performance, we estimated female time to pregnancy based on retrospective
257 husbandry records. We generated a null distribution of time to conception which demonstrates
258 distinct periodicity corresponding to the mouse female estrous cycle lasting 4-5 days (**Figure**
259 **4E**). Next, we stratified our population by maternal genotype. For *Csmd1* wildtype mothers, the
260 bulk of conceptions occurred within the first estrous cycle as expected (Foldi et al., 2011),
261 whereas most *Csmd1* knockout mothers became pregnant after two or more cycles ($\beta_{GT} = 10.4$; P
262 = 0.012). A small minority of knockout females required many cycles to achieve pregnancy (>
263 60 days). Circulating gonadotropin levels did not differ between wildtype and knockouts after
264 controlling for estrous stage, suggesting that this reduction in mating success was not secondary
265 to impaired hormonal input along the HPG axis (**Methods**, **Figure S4**). Instead, if *Csmd1*
266 knockout females bear a reduced ovarian reserve, there may be a reduced probability of
267 conception per cycle due to a smaller oocyte target for male sperm. Interestingly, while knockout
268 females achieved fewer pregnancies per estrous cycle, the average number of offspring born per

269 pregnancy did not differ significantly between wildtype and knockout mothers ($\bar{x}_{wt}$ = 6.6 (95%
270 CI [5.4-7.8]); $\bar{x}_{ko}$ = 6.9 (95% CI [5.7-8.1]); **Figure 3D**). However, pups borne of *Csmd1*
271 knockout mothers suffered from significantly higher mortality rates during the neonatal period (1
272 - 10 days) when compared to wildtype/heterozygous mothers (% $\text{mortality}_{WT/het}$ = 10.5% (95%
273 CI [3.6% - 17.5%]); % mortality_{KO} = 50.0% (95% CI [30.0% - 70.0%]); Poisson regression P =
274 7.93×10^{-7}; **Figure 5A**). We performed necropsy on expired offspring which revealed an absence
275 of milk spots, suggesting death by starvation. Because neonatal mortality segregated with
276 maternal genotype but not offspring genotype or paternal genotype, we hypothesized that this
277 increase in mortality could be explained by a nursing defect in *Csmd1*-deficient mothers.
278 Therefore, we performed IF to confirm that CSMD1 is expressed in the normal mammary gland
279 through the adult life cycle of wildtype animals (**Figure 5B**). CSMD1 is observed on both
280 luminal epithelial cells and myoepithelial cells of the mammary ducts, and on numerous stromal
281 cells (**Figures 5B** and **5C**). Ductal cell expression of CSMD1 appears to be regulated throughout
282 the life cycle, with lowest expression seen in virgins, increasing in mid-pregnancy and lactation,
283 with maximal expression during involution. Mammary glands from knockout females showed
284 reduced density of the epithelial branching network during mid-pregnancy and post-nursing,
285 likely explaining the lack of milk available to nursing pups (**Figure 5D**). Visual comparison of
286 duct morphology in nulliparous wild type and knockout animals suggested that the main
287 structural defect was a highly reduced incidence of lateral branches prior to pregnancy (**Figure
288 5E**), a conclusion that was statistically supported by quantitative image analysis (**Figure 5F**).

289 **The complement pathway is dysregulated in *Csmd1* knockout mice**

290 The primary protein sequence of *CSMD1* shares homology with complement-interacting proteins
291 (Kraus et al., 2006). Complement acts as an inflammatory/phagocytic signal in the innate immune

292 system (Liszewski et al., 1996), and recent work has shown that classical complement components
293 C1q and C3 are also responsible for microglia-mediated phagocytosis of excess neuronal cells in
294 a normal developmental process known as synaptic pruning (Schafer et al., 2012). *CSMD1*
295 (Schizophrenia Psychiatric Genome-Wide Association Study, 2011) (Schizophrenia Working
296 Group of the Psychiatric Genomics, 2014) and complement *C4* (Sekar et al., 2016) have also
297 been associated with schizophrenia in independent, well-powered human association studies.
298 Furthermore, some of the most significantly associated variants previously associated with
299 azoospermia encompass the greater MHC locus, which include complements *C2*, *C4* and factor
300 B (Ni et al., 2015; Zhao et al., 2012). *Csmd1* is also known to inhibit the classical complement
301 pathway *in vitro* (Escudero-Esparza et al., 2013; Kraus et al., 2006). Thus, to consolidate the putative
302 roles of complement with *Csmd1*-mediated pathology, we investigated the activity of
303 macrophages and complement component C3 in wildtype and *Csmd1*-null gonads. *C3* mRNA is
304 detectable in whole testes and ovaries, and in testicular germ cells at multiple stages of
305 spermatogenesis (**Figure 6A**). *C3* and *Csmd1* mRNA expression are anticorrelated throughout
306 spermatogenesis. Macrophages, the immune cells most commonly associated with complement-
307 mediated phagocytosis, are found in the interstitial space between seminiferous tubules (**Figure**
308 **6B**). We frequently observed C3 in the interstitial space, but not within the tubules; likewise, C3
309 could be observed further downstream in the epididymis, in the peritubular regions but not inside
310 the lumen (**Figure 6B**). We measured bulk macrophage content and complement C3 deposition
311 in *Csmd1* wildtype and knockout testes (**Figure 6C; Figure S5; Methods**). The proportion of
312 C3-positive cells is significantly higher in *Csmd1* knockout versus wildtype testes ($\bar{x}_{wt}$ = 0.017;
313 $\bar{x}_{ko}$ = 0.066; ANOVA P = 7.7 x 10^{-4}), consistent with an inhibitory role for *Csmd1* against
314 complement.

315 In wildtype ovaries, we observed a localization of C3 and macrophages that support the
316 hypothesis that complement-mediated phagocytosis and cellular remodeling are processes that
317 regulate normal gonadal function. Interestingly, C3 is localized to the oocyte surface in normal
318 developing follicles, colocalized with CSMD1, and then observed to be diffused in large
319 amounts throughout the corpus luteum, which is devoid of CSMD1 (**Figures 6D and 6E**).
320 Macrophages are a prominent cell type in the ovary and associated with, but excluded from
321 entering, healthy follicles; they invade corpora lutea and degrading follicles (**Figure 6E**). As
322 predicted in a model of C3-mediated phagocytosis by macrophages, C3 colocalizes with
323 macrophages in the corpus luteum as well as in atretic follicles. Interestingly C3 is abundant
324 within the early follicular antrum (probably in follicular fluid), suggesting that C3 may be
325 important for remodeling the connections between granulosa cells during antrum formation
326 (**Figure 6E**). It has previously been reported that activated C3 is present in human follicular fluid
327 at levels comparable to sera, but its physiological role in folliculogenesis, ovulation or
328 fertilization is unknown (Perricone et al., 1992).
329
330 Finally, we observed a pattern of C3 and CSMD1 expression in wildtype mammaries that also
331 supports the notion that CSMD1-complement interactions are dysregulated in the pathologies
332 observed in CSMD1 knockouts (**Figure 6F**). As early as puberty, C3 can be seen in high levels
333 within the mammary duct lumen of virgin animals. We speculate that C3 may be involved in the
334 process of lumen formation, as lower levels of C3 are observed in lumens that are just beginning
335 to open and contain dissociated cells. C3 is also expressed within vesicles of specific subsets of
336 CSMD1-positive stromal cells, likely macrophages or eosinophils.

337 Based on previous findings that CSMD1 is a negative regulator of C3, we predicted that removal
338 of C3 would partially or completely alleviate the morphological degeneration and fertility defects
339 observed in *Csmd1* knockout mice. To test this prediction, we generated a colony of *C3/Csmd1*
340 double knockout (DKO) mice. Surprisingly, we found no evidence of rescue in DKO males or
341 females (**Figure S6**). Instead, we observed an unmasked phenotype of more severe histological
342 degeneration in all DKO females, characterized by even more invasion of foam cell
343 macrophages, extensive pyknosis, and deformed follicles. We also observed profound
344 inflammatory changes in the mucosal layer of the oviduct (**Figure S6B**). We monitored the
345 fertility of 19 DKOs (10 males and 9 females), and of these, only 4 (21%) produced progeny
346 after at least 3-7 months of mating (3 males and 1 female; **Table S3**, **Figure S6C**). The average
347 litter size resulting from successful mating was small compared to wildtype (mean size 4.25
348 pups). These extreme phenotypes are not observed in *Csmd1* nor *C3* single knockouts, indicating
349 that the combined effect of *Csmd1* and *C3* on fertility is synergistic.
350

351 ## Discussion

352

353 We used a human genetic screening approach to identify genes that modulate male and female
354 gonadal function, and identified a strong candidate, the complement regulator *CSMD1*. The
355 human phenotypes that we studied were ascertained for having abnormal, early loss of germ cell
356 development, and we observed defects in gametogenesis in both male and female *Csmd1*
357 knockout (KO) mice. We performed a series of experiments with mice to evaluate three
358 competing explanations for this germ cell loss: increased cell death, failure of proliferation, or
359 increased phagocytosis.

360

361 During our work-up of testis pathology in sexually mature *Csmd1*-null mice, we observed neither
362 qualitative nor quantitative differences in the abundance of apoptosis markers TUNEL in testis
363 cross sections or Annexin-V in dissociated whole testis FACS (data not shown). These
364 observations, coupled with adult onset of the testes degeneration phenotype do not support an
365 increase in apoptosis as the mechanism for gonadal dysfunction.

366

367 Because much of the hormonal and cellular machinery for cell division is shared between both
368 sexes, a failure of proliferation either due to endocrine disruption or maturation arrest is another
369 possible explanation for infertility in males and females. We excluded systemic endocrine
370 defects that would be observed in the case of failure of the hypothalamus or pituitary (**Figure**
371 **S4**). We did not observe any stage-specific accumulation or depletion of germ cells in either sex,
372 nor, as mentioned above, any tell-tale signs of excess apoptosis that is usually seen in such cases
373 (Lipkin et al., 2002; Yatsenko et al., 2015). We observed no significant differences in PCNA marker
374 levels between *Csmd1* wildtype and knockout testes of adult animals (data not shown).

375

376 The finding of increased C3 deposition in testis, coupled to the known complement-regulatory
377 function of CSMD1, suggests that improper phagocytosis of cells or cellular structures underlies
378 at least part of the defect, but does not illuminate the cell type(s) or biological process(es) that
379 are consequently affected. The diverse defects observed by histology points to a problem in
380 maintenance of the stem cell niche or stem cell function, and possibly Sertoli cell function. We
381 see no consistent signs of defects in germ cell morphology or stage-specific depletion or
382 enrichment of cells. There were no overt signs of derangement of Sertoli cell phagocytosis, such

383 as a universal bloating of Sertoli cell vacuoles, or the abnormal presence of elongated spermatid
384 heads near the basement membrane, in all *Csmd1* KOs investigated. We observed no evidence of
385 complement deposition inside the lumen of the seminiferous tubules. It is widely believed that
386 the tubules are an immune privileged site, and we observed no evidence of macrophages inside
387 the tubules or disruption of the blood-testis-barrier (BTB) in knockouts. However, both
388 spermatogonial stem cells and Sertoli cells exist outside the BTB, and macrophages have been
389 shown to be required for proper SSC differentiation (DeFalco et al., 2015). In further support of
390 a niche defect, the strongest quantitative difference in protein abundance observed between
391 wildtype and *Csmd1* KO, among over 20 proteins tested, was a universally lower expression of
392 the germ cell nuclear antigen TRA98 in spermatogonia (**Figures 3D and S3D**). Our results are
393 also consistent with a role for Sertoli cells in the pathology of knockouts, either due to
394 interactions with germ cells or interstitial cells, as we see extensive sloughing of germ cells from
395 the epithelium, as well as rare whorls of Sertoli cells in the lumen (**Figure 3B**).
396
397 The histology data from ovaries are consistent with a model where dysregulation of the
398 macrophage-complement axis leads to loss of developing follicles and/or oocytes. Macrophage
399 activity in the ovary is very carefully regulated in time and space during the estrous cycle. It is
400 well known that macrophages are physically associated with most if not all developing follicles,
401 and that this association is not just a response to atresia (Gaytan et al., 1998; Tingen et al., 2011).
402 After ovulation, macrophages invade the ruptured follicle which undergoes apoptosis/phagocytic
403 luteolysis, forming the corpus luteum (Kato et al., 2005). CSMD1 is also highly expressed on
404 oocytes of the developing follicle, but not in the corpus luteum (**Figure 2E, F**). Disruption of
405 CSMD1 function may allow for premature macrophage invasion of the developing follicle,

406 leading to excessive oocyte atresia, fewer ovulations, and reduced probability of pregnancy
407 (**Figure 4D,E**). *Csmd1* null females give birth to normal litter sizes, which limits the possibility
408 that CSMD1 mediated follicle loss occurs during the cyclic recruitment of antral follicles.
409 Instead it may be operating at the phase of initial recruitment, or perhaps even earlier in the
410 establishment of the oocyte or follicle pool. A more sensitive analysis of oocyte and follicle
411 counts at multiple time points will be needed to pinpoint exactly where in the oocyte lifecycle
412 atresia occurs.
413
414 In addition to the gonads, *CSMD1* also governs post-natal developmental processes across other
415 tissue systems. We have demonstrated a robust association between neonatal mortality rate and
416 maternal *Csmd1* genotype status, with corresponding reduction in the epithelial network of the
417 maternal mammary gland (**Figure 5**). The mammary gland is a highly motile network of
418 branching epithelial tissue that advances and recedes during different stages of post-natal
419 development (i.e., puberty, pregnancy, nursing, etc. (Sternlicht, 2006)). The characteristic
420 directionality of mammary branching is conferred by polarized cell proliferation and
421 phagocytosis mediated by macrophage remodeling, especially in anticipation of nursing (Pollard,
422 2009). Furthermore, multiple complement and complement-regulatory components are robustly
423 upregulated during periods of apoptosis and phagocytosis in the mammary tissue of multiple
424 species including humans (Clarkson et al., 2004; Laufer et al., 1999), though the functional
425 significance of this regulatory pattern is unknown. Breast milk itself also suppresses complement
426 activation (Ogundele, 1999). Finally, CSMD1 is expressed on the luminal aspect of mammary
427 ducts and terminal end buds, where much of the pregnancy-associated breast remodeling occurs
428 (**Figure 5B**) (Kamal et al., 2010; Kraus et al., 2006). We show a reduction in mammary

429 epithelial density, due to reduction in secondary or tertiary branch points, whose normal geneses
430 are governed by multiple up- and down-regulatory chemotactic signals in concert with physical
431 interaction with phagocytic immune cells (i.e., macrophages)(Ingman et al., 2006)
432
433 It is possible to propose a model to reconcile the pathology that we observe across multiple
434 tissues in *Csmd1* null animals. While complement has a well-appreciated role in innate
435 immunity, evidence is beginning to emerge that it plays a role in the regulation of self cells
436 during normal human development. A key example of this biology is the recent description of
437 complement-mediated synaptic pruning in the developing brain, a process that is under genetic
438 influence and can confer risk for disease when dysregulated (Schafer et al., 2012; Sekar et al.,
439 2016). Here, we have reported complement-associated pathology of post-natal developmental
440 processes in three additional tissues in *Csmd1* null animals; we have observed complement
441 protein expression in all three tissues, and macrophages have been shown to be essential for
442 normal development in all three tissues. A parsimonious model to describe the set of defects we
443 observe here is that macrophages (and perhaps other phagocytes) regulate and refine developing
444 cells in testis, ovaries, and mammary by controlled deposition of complement onto their cell
445 surface.
446 In this model, differentiating cells that progress through developmental checkpoints upregulate
447 complement regulators on their cell surface. Healthy, well-formed cells (including
448 macrophages) secrete C3 at low level continuously into interstitial space and possibly onto the
449 surface of cells. A function of this local complement synthesis is low grade activation to get rid
450 of "junk," without an adaptive immune response or very vigorous innate one. Intracellular and
451 extracellular C3 is available to tag and mark unwanted cells or cell-derived structures for

452 removal. CSMD1 (and presumably other complement regulators) has a special function that
453 involves complement modulation at a highly localized and specific immune privileged site. A
454 certain amount of activated C3 fragments need to be deposited on a target to carry out a specific
455 function – too much or too little has a "bad" consequence. We call this controlled phenomenon
456 targeted and restricted activation of the complement system (TRACS), and initially described the
457 concept of TRACS to explain the function of the complement regulator membrane cofactor
458 protein (MCP) in controlling complement deposition on the inner acrosomal membrane of
459 acrosome-reacted spermatozoa (Riley-Vargas et al., 2005).
460 In our model, there is normally limited or no engagement of adaptive immune players who are
461 not present near the site of TRACS and require more of an acute inflammatory setting to get
462 there. CSMD1 deficiency may be enough to periodically tip the balance of controlled
463 complement activation towards a pathogenic outcome. Conversely, if debris is not removed,
464 developmental processes are disorganized or blocked. In this way, C3 inactivation is predicted to
465 exacerbate, not rescue, the fertility defects we observed in *CSMD1* null animals. If complement
466 marks targets of phagocytosis in the testis as previously shown in the brain, ectopic complement
467 expression across the BTB may inappropriately activate the apoptotic and phagocytic apparatus
468 in *Csmd1* KO testes. Remarkably, *TEP1* (a distant ortholog of *C3*) has been shown to clear
469 apoptotic germ cells in the mosquito testis by this very process (Pompon and Levashina, 2015) .
470 The TRACS model is consistent with known molecular functions of macrophages and
471 complement. However, macrophages have recently been shown to regulate the spermatogonial
472 stem niche by an unknown molecular mechanism (DeFalco et al., 2015). The defects we observe
473 in CSMD1 -/- males are consistent with a niche problem, and we speculate that controlled
474 complement deposition on spermatogonial cells could mediate interactions with macrophages.

475

476 The unmasking of a more severe phenotype in *C3/Csmd1* DKO mice is an unexpected but
477 previously documented signature of complement-mediated disease. For example, double
478 knockout of complement factor H (*CFH*) and factor P (*CFP*) unexpectedly converts mild C3
479 glomerulonephritis to lethal C3 glomerulonephritis in mice(Lesher et al., 2013). Similarly
480 *CFH/C3* DKO unexpectedly unmasks a more severe form of age-related macular degeneration in
481 mice(Hoh Kam et al., 2013). Multiple explanations for this phenomenon have been set forth,
482 including a dual role of C3, differences between fluid-phase and local C3 activation, and C3 gain
483 of function. More extensive mutation constructs including conditional knockouts and allelic
484 series may help to distinguish among these scenarios.

485

486 Finally, we note that our observations may be informative about the biological basis for the
487 highly elevated mutation rate over *CSMD1*. Recently, it has been reported that the two hottest
488 hotspots for maternally derived DNMs in humans are centered on two large genes: *CSMD1* and
489 *WWOX* (Goldmann et al., 2016). These two genes are also among the top 27 most frequent sites
490 of double-strand break formation in primary neural progenitor cells(Wei et al., 2016). Careful
491 study of CNV mutation mechanisms has led to a specific model for the genesis of CNVs over
492 large genes, known as Transcription-dependent Double-Fork Failure (TrDoff), whereby
493 transcription of large genes interferes with DNA replication (Wilson et al., 2015). The TrDoff
494 model predicts that duplications will be enriched at the edges of large gene, while deletions are
495 enriched in the gene body, a pattern that is consistent with our data on *CSMD1* (**Figure 1B**). We
496 have observed that CSMD1 protein is present in primordial follicles of adult mice, suggesting
497 that *CSMD1* is transcribed in oocytes throughout most, perhaps all, of the life of the animal. We

498 predict that this constant, sustained transcription of a large gene in each oocyte may expose the
499 female germline to transcription-coupled molecular conflicts like TrDoff that are not as
500 pronounced in the male germline. We speculate that this could be exacerbated by incomplete
501 DNA replication at *Csmd1* at the time that the oocytes arrest in MI, and differences in the
502 amount of replication stress experienced during the initial expansion of the germ cell pool, which
503 happens more quickly in females compared to males. We predict that the *WWOX* is also
504 expressed in oocytes with a developmental timing similar to *CSMD1*.
505
506 In conclusion, we have used human genetics and animal models to identify a likely role for the
507 complement system in postnatal developmental processes across multiple tissues in the body.
508 When combined with existing observations from mammalian brain and other model organisms,
509 we predict that macrophage mediated complement activity on self cells is a normal and highly
510 controlled process in many developmental systems in metazoans. Our work highlights the need
511 for deeper investigation into the role of immune system components in reproductive tissues, and
512 the opportunities that such work can have to illuminate and connect common biological
513 processes that produce disease in more complex contexts across the body.

514 Materials and Methods

515 Human Patient Populations

516
517 We used male infertility case-controls cohorts that were previously described (Huang et al.,
518 2015; Lopes et al., 2013).
519 **WHI-SHARe.** To create an analogous case-control cohort of female gonadal dysfunction, we
520 turned to the SNP Health Association Resource (SHARe) cohort studied under the umbrella of

521 the Women's Health Initiative (WHI)(Hays et al., 2003). We constructed POI case and control
522 definitions from the dense reproductive phenotype data collected on each subject. A self-reported
523 age of menopause before 40 years was used as the only case inclusion criterion. Case exclusion
524 criteria were oophorectomy prior to age 40, a diagnosis of lupus or rheumatoid disease, and a
525 "yes" answer to the question "Did a doctor ever say that you had cancer, a malignant growth, or
526 tumor?". Smoking history, which is a known factor influencing ovarian reserve, was controlled
527 for during the analysis of genetic data.

528 **UK Biobank.** We generated a table of phenotype data for constructing POI case and control
529 labels using controlled-access data from the UK Biobank. Exclusion criteria for the study were:
530 withdrawn consent, poor heterozygosity or missingness as defined by the UK Biobank; > 10
531 relatives in the UK Biobank cohort; not used in autosome phasing, apparent sex chromosome
532 aneuploidy; mismatch between genetic and self-reported sex; ever smoker; any self-reported
533 non-Caucasian ancestry; prior diagnosis of rheumatoid arthritis, lupus, or pelvic cancer;
534 mismatch between self-reported ethnicity or age at menopause among three assessments; SNP
535 array call rate <98%. In the case of pairs of 2nd degree relatives or closer, the one individual with
536 the lower SNP-call rate was dropped. The inclusion criteria for POI case status were self-
537 reported age of menopause < 40 years old, and all remaining individuals in the cohort (after
538 exclusions mentioned above) were used as controls.

539 **Parent-Offspring Trios.** For estimation of chromosome 8 human *de novo* mutation rates, blood
540 samples were collected from parent-offspring trios, parent-twin quartets, and parent-triplet
541 quintets who delivered at Inova Fairfax Hospital and whole genome sequence data were acquired
542 as part of the Inova Translational Medicine Institute's Premature Birth Study as described
543 previously (Goldmann et al., 2016).

544 ## Mouse colony breeding

545

546 We acquired a constitutive *Csmd1* knockout mouse (*Mus musculus)* on a mixed
547 129SvEvBrd:C57BL/6 background from the UC Davis KOMP Repository (Project ID
548 CSD118901). The original construction of the mouse is described previously(Friddle et al.,
549 2003). Briefly, a 1.086 kb deletion encompassing *Csmd1* exon 1 and part of intron 1 were
550 replaced with a lacZ/neomycin cassette. Deletion of this segment was confirmed with Southern
551 blot and PCR. Due to the extreme size of *Csmd1* (1.6 Mb), we also analyzed RNA seq data
552 across all 70 exons in knockout testes and ovaries. In ovaries, knockout read counts relative to
553 wildtype are suppressed across all 70 exons. In testes, knockout read counts relative to wildtype
554 are broadly suppressed across exons 1-57 and upregulated from exons 58-70. The amino acid
555 coding portion of these upregulated exons range in size from 45 bp to 180 bp. The translational
556 viability of these fragments is unknown. All littermate tissue comparisons in this study
557 (described below) were generated from $dam_{heterozygous}$ x $sire_{heterozygous}$ crossings from this original
558 colony. Next, to eliminate variance in phenotype explained by variance in background genotype
559 (if any), we serially backcrossed the *Csmd1* mutation onto a constant C57BL/6 background for 5
560 generations. From this F5 backcross generation we performed a $dam_{heterozygous}$ x $sire_{heterozygous}$
561 cross from this to create wildtype and knockout littermates, and performed analogous histology
562 and immunofluorescence experiments as with the original colony (described below; **Figure S7**).
563 We performed microsatellite genotyping of these littermates to estimate the C57BL/6
564 background after backcrossing (Washington University Rheumatic Disease Core). We estimated
565 the F5 proportion of C57BL/6 ancestry of 0.91 (95% CI [0.89-0.93]). For DKO experiments, we
566 introgressed a *C3* mutant line described previously (Circolo et al., 1999) until we achieved
567 *Csmd1/C3* DKO mice.

568

569 ## CNV and SNV discovery

570

571 Array data for the Women's Health Initiative SHARe cohort were downloaded from the NCBI
572 Database of Genotypes and Phenotypes (dbGAP accession number phg0000g1.v2). SHARe
573 samples were genotyped on the Affymetrix 6.0 platform. We created a high-quality set of CNV
574 calls for all cohorts using our own internal pipelines. SHARe samples were processed with
575 Affy6CNV (a wrapper that we wrote for the Birdsuite package (Korn et al., 2008)) for data
576 processing and QC. We obtained raw SNP array data from the UK Biobank and performed
577 single sample CNV discovery using PennCNV(Wang et al., 2007). Individuals with > 200 CNV
578 calls were dropped. CNV calls with PennCNV quality score > 30 were retained, and adjacent
579 CNVs in the same sample were merged.
580 Exome sequencing was performed on a subset of the WHI subjects as part of the Women's
581 Health Initiative Sequencing Project (WHISP); all available WHISP BAM files were
582 downloaded from the NCBI Database of Genotypes and Phenotypes (dbGaP accession
583 phs000200.v10.p3.c1 and phs000200.v10.p3.c2)(Tryka et al., 2014). Genotypes were recalled,
584 jointly, from 1,668 WHI BAM files using Haplotype Caller, recalibrated and cleaned according
585 to GATK best practices using GATK-3.2.2.

586 ## Association testing

587

588 **CNVs.** Rare CNVs were associated with case-control status using generalized linear models. For
589 the SHARe association analysis, we included the top 10 ancestry eigenvectors (calculated from
590 the full SHARe genotype matrix) and smoking history as covariates. For the UK BioBank

591 association analysis, individuals with any history of smoking were excluded from the analysis,
592 and we included as covariates BMI and the top 10 ancestry eigenvectors calculated from the full
593 UK Biobank SNP genotype matrix.
594 **SNVs.** We tested for an association between rare SNVs in *CSMD1* and age at menopause in the
595 WHI samples using the Sequence Kernel Association Test (SKAT) (Lee et al., 2012), weighting
596 each variant with the Combined Annotation Dependent Depletion (CADD) value (Kircher et al.,
597 2014). Five ancestry eigenvectors and smoking history were included as covariates; significance
598 was evaluated using bootstrapping with 5,000 samples.
599

600 ## Testes dissociation, cell sorting, and RNA extraction
601
602 Sexually mature (40 ± 1 days old), wildtype male mice were sacrificed, and their testes were
603 decapsulated and homogenized in a 1X MEM solution (Gibco 11430-030) containing 120 U/mL
604 Type I Collagenase (Worthington Biochemical LS004194) and 1 mg/mL DNAse I (Roche
605 10104159001), and agitated for 15 minutes. 1X MEM was replaced and added with 50 mg/mL
606 Trypsin (Worthington Biochemical 54J15037) and 1 mg/mL DNAse I and agitated for 15
607 minutes, then mechanically homogenised for 3 minutes. 50 mg/mL Trypsin and 1 mg/mL
608 DNAse I were added and agitated again for 15 minutes. We added 0.4 mL heat inactivated Fetal
609 Bovine Serum (Sigma F1051), 5 µL Hoescht 33342 (Life Technologies H3570), and 1 mg/mL
610 DNAse I, and agitated for 15 minutes. Individual cells were dissociated by pipetting sequentially
611 through two 40 µm cell strainers (Falcon 352340). For each individual mouse, one dissociated
612 testis was used for wholetissue RNA extraction and sequencing, and the other testis was used for
613 germ cell purification, RNA extraction, and sequencing. All dissociation steps were performed at
614 33°C. Dissociated testes were sorted as described previously on a modified MoFlo cytometer

615 (Beckman Coulter) at the Washington University Siteman Flow Cytometry Core using a
616 krypton-ion laser (Lima et al., 2016). Cells that are stained with Hoechst can be clustered in two
617 wavelengths: (i) blue fluorescence, which is informative of DNA content, and (ii) red
618 fluorescence, which is informative about chromatin state and Hoechst efflux from the cell. Based
619 on these parameters, we separated homogenised testes suspensions into four purified
620 populations: (i) spermatogonia, (ii) primary spermatocytes, (iii) secondary spermatocytes, and
621 (iv) spermatids. These separated populations were collected and RNA extraction performed on
622 them. RNA from whole testes was extracted with the RNeasy Plus Mini Kit (Qiagen 74134), and
623 RNA from FACS-purified germ cell populations was extracted with the RNeasy Plus Micro Kit
624 (Qiagen 74034).
625

626 ## RNA-seq
627
628 Whole testis, whole ovaries, and purified male germ cell subpopulations were obtained from
629 wildtype and *Csmd1* null siblings. We extracted polyadenylated mRNAs from each tissue/cell
630 type and converted these into RNA-seq libraries. Three biological replicates of each tissue or cell
631 type were sequenced with a 2 x 101bp paired-end protocol. Reads were mapped to Ensembl Mus
632 musculus reference R72 and transcript expression levels were summarized as reads-per-kb of
633 exon per million-mapped reads (RPKM) using the TopHat2 package(Kim et al., 2013). RPKMs
634 were adjusted for batch effects and cryptic covariates using PEER(Stegle et al., 2012), quantile
635 normalized, and then the R package poissonSeq was used for differential expression analyses(Li
636 et al., 2012).

637

638 ## Immunostaining and imaging

639

640 Testes and ovaries were dissected, fixed in 4% paraformaldehyde (Electron Microscopy
641 Sciences), and embedded in paraffin. We baked 5μm sections at 60°C for 1 hr, deparaffinized in
642 Xylenes, and rehydrated into PBS (Corning). Antigen retrieval was done in boiling citrate buffer
643 (10mM sodium citrate, 0.05% Tween-20, pH 6.0) for 20 min. Sections were blocked in PBS
644 containing 0.2% Triton X-100 and 5% normal donkey serum (Jackson Laboratories) for 1 hr at
645 room temperature and then incubated with primary antibodies diluted in blocking solution over
646 night at 4°C. After washing with PBS-Tx (PBS containing 0.2% Triton X-100), they were
647 incubated with fluorescent secondary antibodies in blocking solution for 1 hr at room
648 temperature, washed with PBS-Tx, and treated with 0.2% Sudan Black in 70% EtOH for 10 min,
649 followed by PBS washes. The sections were then counterstained with Hoechst dye 33342
650 diluted 1:500 in PBS for 5 min, washed once with PBS-Tx for 2 min and then with PBS, and
651 mounted in ProLong Diamond anti-fade mounting medium (Molecular Probes). Imaging was
652 done on an Olympus LSM700 confocal microscope using Zen software, and images were
653 processed using Photoshop CS5 (Adobe). Antibodies used were gt α-CSMD1 N20 (Santa Cruz
654 Biotechnology, 1:100), rb α-mouse vasa homolog (MVH) (Abcam 13840, 1:1,000), donkey α -gt
655 CF594 (Biotium, 1:300), and donkey α -rb Alexa488 (Life Technologies, 1:300), rb α- β-gal
656 (Cappel 1:333), rat F4/80 BM8 (Santa Cruz Biotechnology 1:50), donkey α -rat Alexa488 (Life
657 Technologies, 1:300), rb α-C3 (Abcam 200999, 1:2,000), and gt α-rb Alexa568. Whole mount
658 IF samples were prepared as described previously (DeFalco et al., 2015). For
659 immunohistochemistry, 5μm paraffin sections were treated as above, except the secondary
660 antibody was biotin-coupled horse α-goat (Vector Laboratories, BA-9500, 1:200), and detection

661 was done using the Vectastain Elite ABC kit (Vector Laboratories, PK-6100) and DAB
662 Peroxidase Substrate kit (Vector Laboratories SK-4100) per the manufacturer's instructions.
663 Sections were counterstained with hematoxylin, mounted in Cytoseal Xyl (Thermo Scientific),
664 and imaged on a Zeiss Axioplan 2 microscope equipped with an Olympus DP71 camera and DP
665 software. X-gal staining was performed as described previously (Li et al., 1998) .

666

667 ## Histology

668

669 Freshly-dissected gonads were fixed under agitation in Modified Davidson's fixative (Electron
670 Microscopy Sciences 64133-50) for 24 hour and Bouin's fixative (Electron Microscopy Sciences
671 26367-01) for 24 hours. Fixed tissues were embedded in paraffin and sectioned at 5 μm.
672 Sectioned tissues were stained with hematoxylin and counter-stained with eosin. Stained testes
673 from 65 individual mice of known age and genotype (12 wildtype, 53 knockout) were provided
674 to a single mouse pathologist in a blinded fashion. All samples received a score of 0 (no
675 damage), 1 (mild damage), or 2 (profound damage) (see **Figure S3A** for examples). In order to
676 estimate the effect of genotype on score, we fit a linear analysis of variance model:

677 $y_{ijk} = \mu + \alpha_i + \beta_j + \varepsilon_{ijk}$ [1]

678 where y_{ijk} is the damage score for individual *k*, μ average damage score across all animals, α_i is
679 the effect of genotype *i*, β_j is the effect of age *j*, and ε_{ijk} is the random error associated with the
680 *k*th observation.

681 ## Germ cell quantification

682

683 We performed immunofluorescence as described above on a pair of 34 day old male littermates
684 (the same individuals as seen in **Figure 3A**) using anti-TRA98 antibody (Abcam ab82527). We
685 generated count data for total cells (filtering based on size and shape), and for TRA98-positive

686 cells (filtering based on green fluorescence) using the ImageJ software package. In order to
687 estimate the effect of genotype on TRA98 cell count, we fit the following linear model:
688 $\ln(y_i) = \beta_0 + \beta_1 X_{1i} + \beta_2 X_{2i} + \varepsilon_i$ [2]
689 Where y_i is the TRA98-positive count in image *i*, and X_1 is the genotype (*Csmd1* wildtype versus
690 knockout), and X_2 is the total cell count. ε_i is the nuisance variable for image *i*.

691 ## Gonad size analysis
692

693 We sacrificed 229 adult mice (106 males and 123 females), and measured body weights and
694 bilateral gonad weights at necropsy. For males, mean body weight was 37.1g, mean testes weight
695 was 273mg, and mean age was 201 days. For females, mean body weight was 31.3g, mean ovary
696 weight was 32mg, and mean age was 234 days. In order to estimate the effect of genotype on
697 gonad weight, we fit the following linear model:
698 $y_i = \beta_0 + \beta_1 X_{1i} + \beta_2 X_{2i} + \beta_3 X_{3i} + \varepsilon_i$ [3]
699 Where y_i is the gonad weight in individual *i*, and X_{1i}, X_{2i}, and X_{3i} are the genotype, age, and
700 body weight of individual *i*, respectively. ε_i is the nuisance variable for individual *i*.

701 ## Follicle count analysis
702
703 We sacrificed 15 sexually mature female mice, of which 10 were wildtype and 5 were knockout
704 genotypes. Bilateral ovaries were fixed, sectioned to 5 μm, and stained with H&E. We performed
705 morphological classification of follicles in both ovaries as described previously (Myers et al.,
706 2004). We identified primordial follicles, primary follicles, secondary follicles, early antral
707 follicles, antral follicles, preovulatory follicles, atretic follicles, and *corpora lutea*. In order to
708 estimate the effect of genotype on gonad weight, we fit the following linear model:
709 $\ln(y_i) = \beta_0 + \beta_1 X_{1i} + \beta_2 X_{2i} + \varepsilon_i$ [4]

710 Where y_i is the number of total oocytes in bilateral ovaries of individual *i*, and X_{1i} and X_{2i} are
711 genotype and age, respectively. ε_i is the nuisance variable for individual *i*.

712

713

714 ## Breeding time analysis

715

716 We compiled comprehensive husbandry information over a period of greater than 1 year
717 corresponding to 151 litters born representing all possible *Csmd1* wildtype, heterozygote, and
718 knockout sire/dam breeding combinations. We calculated the number of days between first
719 sire/dam co-habitation and birth of each litter. Next we subtracted an estimated C57BL/6
720 gestation time of 19 days (Murray et al., 2010) to estimate time to conception. We also
721 calculated parental ages at conception. All density plots depicted in **Figure 4** reflect estimated
722 time to conception for all 151 litters. In order to estimate the effect of maternal genotype on
723 mating success, we controlled for paternal genotype by including wildtype sires only. We then fit
724 the following linear model:

725 $y_i = \beta_0 + \beta_1 X_{1i} + \beta_2 X_{2i} + \beta_3 X_{3i} + \varepsilon_i$ [5]

726 Where y_i is the estimated time to conception for mating pair *i*, X_{1i} is maternal genotype
727 (wildtype, heterozygote, or knockout), X_{2i} is maternal age at conception, and X_{3i} is paternal age
728 at conception. ε_i is the nuisance variable.

729

730 ## Litter size analysis

731

732 We bred 44 females (8 wildtype, 27 heterozygote, and 9 homozygote) with 41 males (4 wildtype,
733 26 heterozygote, and 11 homozygote) over a period of 10 months to produce 99 litters, totaling

734 688 live births. All 9 parental genotype permutations [wt_{dam} x wt_{sire}, wt_{dam} x het_{sire} … hom_{dam} x
735 hom_{sire}] were represented multiple times (excepting het_{dam} x wt_{sire}). We counted deaths in during
736 the neonatal period (defined as 1-10 days by convention, although the vast majority of deaths
737 occurred within 24-48 hours) and subtracted from the live birth total to obtain the final number
738 of surviving pups (550 total). Next, we stratified each litter by maternal and paternal genotype
739 status (*Csmd1* wildtype or heterozygous versus knockout) and fit the following linear model:
740 $\ln(y_i) = \beta_0 + \beta_1 X_{1i} + \beta_2 X_{2i} + \varepsilon_i$ [6]
741 Where y_i is the number of surviving pups in litter *i*, and X_{1i} and X_{2i} are the maternal and paternal
742 genotypes, respectively. ε_i is the nuisance variable for litter *i*.
743

744 ## Mammary gland whole-mount analysis

745 Female littermates were collected at four developmental time points: (i) pre-pubescent (< 30
746 days of age); (ii) adult virgins; (iii) mid-pregnancy (estimated 14 days after copulation); (iv)
747 post-weaning (7 days after weaning pups from mother's nursing). Freshly-dissected whole
748 inguinal mammary glands were fixed overnight in Carnoy's solution (60% ethanol, 30%
749 chloroform, 10% glacial acetic acid). Fixed tissues were washed and rehydrated in ethanol and
750 water and stained in Carmine alum histological stain (0.5% Aluminium potassium sulphate,
751 0.2% Carmine) for 48 hours. Stained tissues were dehydrated with increasing concentrations of
752 ethanol and stored in xylene to clear lipids for 48 hours. Finally, tissues were flattened
753 mechanically and suspended in pure methyl salicylate prior to imaging. Due to the large size of
754 whole mammary tissues, overlapping fields of view were captured and stitched together using
755 the "Photomerge" function in Adobe Photoshop. Gaps in the backdrop of the merged images
756 were filled using the "Content aware fill" function in Adobe Photoshop—if and only if the gaps

757 did not overlap any portion of the tissue proper. All original images are available on the Conrad
758 Lab website (http://genetics.wustl.edu/dclab/lee_et_al_images). To perform statistical
759 comparison of duct morphology between genotypes, measurements of mammary gland ducts
760 were derived from images using AngioTool64 v0.6a (Zudaire et al., 2011). First, a skeleton
761 representation of the branched duct structure is generated from the input image, which is then
762 used to compute a variety of morphological and spatial parameters for branching
763 characterization. Since this software detects the branches by contrast on a black background, the
764 images of whole mount mammary glands of adult mice were transformed into a compatible input
765 using ImageJ 1.51n.
766

767 ## Hormone measurements
768

769 We collected serum from 9 males (4 wildtype versus 5 knockout; mean age = 103 days) and 16
770 females in the proestrous stage (7 wildtype versus 9 knockout; mean age = 96 days) via
771 submandibular collection. Each wildtype individual was matched with ≥ 1 knockout littermate.
772 Female estrous cycle was determined by vaginal cytology, as described previously(Byers et al.,
773 2012). All blood was drawn at approximately the same time of day, clotted for 90 minutes at
774 room temperature, and centrifuged at 2000 x g for 15 minutes. Samples were stored at -20°C
775 prior to hormone measurements. Male samples were quantified for LH/FSH (EMD Millipore)
776 and testosterone (Immuno-Biological Laboratories Inc), and female samples were quantified for
777 LH/FSH and estradiol (CALBIOTECH), as described by the University of Virginia Ligand
778 Assay and Analysis Core (http://www.medicine.virginia.edu/research/institutes-and-
779 programs/crr/lab-facilities).

780 ## C3 deposition assay

781

782 Testes obtained post-dissection from *Csmd1* knockout and wild-type mice were decapsulated and
783 washed in 1xPBS before mincing. Minced tissue was subjected to enzymatic dissociation as
784 described by us previously (Lima et al, 2016). The crude cell preparation thus obtained was
785 treated with ACK buffer (Life Technologies) for 5 min at room temperature to lyse erythrocytes
786 present if any in the cell preparation. The isolated cells were incubated in α-C3 (B9) primary
787 antibody (Santa Cruz Biotechnology) for 45 minutes at room temperature (RT) diluted 1: 100 in
788 FACS buffer (1x PBS, 5%FBS, 0.1% Sodium azide) along with 10% Fc block (to minimize non-
789 specific binding and background fluorescence) followed by fluorophore tagged secondary
790 antibody (1:250) incubation of 90 mins at RT in the dark with 3 washes of ice cold FACS buffer
791 after each antibody incubation. Flow cytometry was performed with an Accuri C6 cytometer
792 (BD Biosciences).

793 ## *De novo* mutation calling

794

795 Whole genome sequencing and *de novo* mutation calling are described previously (Goldmann et
796 al., 2016). Whole genome sequencing data were generated using the Complete Genomics
797 Platform. All but one individual was excluded from each identical twin set in order to avoid
798 double-counting same set of de novo mutations. After variant calling and QC we identified 2,058
799 DNMs across 709 trios. Finally, in order to assess the discrepancy, if any, between the high
800 frequency of observed mutations about *CSMD1* and the intrinsic mutability of its primary
801 sequence, we calculated a per-nucleotide mutation rate to every base across chromosome 8,
802 based on pre-computed scores for 1,536 five-bp motifs.

803 ## *Sample-size estimation*

804

805 Human genetic studies were carried out using existing datasets, 2/3 of which were generated by
806 large epidemiological studies; thus, we simply used the sample sizes of cases and controls that
807 were available to us. Based on empirical findings for diseases with similar genetic architecture
808 (e.g. autism and schizophrenia) we hypothesized that sample sizes of approximately 500-1000
809 cases and thousands of controls would be sufficient to detect rare, large effect variants such as
810 the 16p11 deletion that has a frequency of ~1% in cases of autism, which was originally detected
811 as associated with only 180-500 cases of autism (Kumar et al., 2008; Weiss et al., 2008). For
812 animal studies, we generated a large colony of wildtype, single and double knockouts that
813 provided all phenotype and tissue data required for analyses. For tissue studies, we assayed at
814 least 6 sections of the tissue of interest from at least 3 independent animals. For quantitative
815 phenotyping, we assayed at least 3 independent animals (biological replicates). For ELISA
816 (hormone assays) and FACS (protein abundance) experiments, a minimum of 3 technical
817 replicates were taken on each animal and averaged.

818

819

820 **Author Contributions:**

821

822 D.F.C. devised the study. A.S.L. and D.F.C. led the experimental design. A.S.L. and D.F.C led
823 the data analysis. A.S.L., A.C.L., N.H., K.A.V., W.S.W.W., R.E.W., J.P.A., and D.F.C.
824 performed data analyses. J.E.N. supervised the data collection and sequencing of the human
825 family trios. A.S.L., J.R., A.U., X.W., and R.A.H. performed experiments. A.S.L. and D.F.C.
826 wrote the manuscript. All authors read and approved the manuscript.

827

828 **Description of Supplementary Data**

829

830 Supplementary Figures- contains 6 supplemental figures and supplemental table.

831 In addition, there are two large tables of data that are provided separately:

832 Table S1 – The full set of CNV calls and inferred POI case/control status that we generated from
833 the WHI SHARe cohort.

834 Table S2 – All deletions detected in introns 1-3 from SHARe, the azoospermia cohort, and UK
835 Biobank, along with case/control status of each deletion carrier.

836 Table S3 – Results of breeding CSMD1 -/- C3 -/- double knockouts. Nineteen double knockouts
837 were bred for 3-7 months. This table contains summary details on the outcome of
838 breeding for each animal, including number of litters born and litter size(s).

839

840 **Conflicts of Interest**
841

842 We declare no competing personal or financial interests.

843

844 **Acknowledgments**
845

846 We thank all patients and study participants. D.F.C is supported by the National Institutes of
847 Health (R01HD078641 and R01MH101810). A.S.L. is supported by a Distinguished Scholar
848 Award from Washington University School of Medicine. The ITMI Premature Birth Study was
849 funded by the Inova Health System. We thank Heather Lawson for training and consultation on
850 animal husbandry. We thank Brianne Tabers for technical assistance with animal husbandry. We
851 thank J. Carlson and S. Zollner for early access to Mr. Eel, software for annotating context-
852 dependent mutation rates. We thank Kelle Moley and members of her laboratory (Praba Esakky,
853 Michaela Reid, and Jessica Saben) for consultations on tissue preparations. We thank Tim

854 Schedl and Nicole Rockweiler for helpful discussions. We thank Nicholas Ho for technical
855 assistance with image quantification. We thank Jakob Goldmann and Christian Gilissen for
856 providing us the software for calling and phasing the de novo mutations in family trio data. We
857 thank Seungeun Lee for discussion of SKAT results. We thank Bill Eades and Chris Holley at
858 the Washington University Siteman Flow Cytometry Core (NCI P30 CA91842) FACS services.
859 We thank the Washington University Rheumatic Disease Core (NIHP30AR48335) for providing
860 backcrossed mouse genotypes. We thank the University of Virginia Ligand Assay and Analysis
861 Core (U54 DH28934) for hormone measurements.

862

863 **References:**

864 Baker, T.G. (1963). A Quantitative and Cytological Study of Germ Cells in Human Ovaries. Proc R Soc
865 Lond B Biol Sci *158*, 417-433.
866 Byers, S.L., Wiles, M.V., Dunn, S.L., and Taft, R.A. (2012). Mouse estrous cycle identification tool and
867 images. PLoS One *7*, e35538.
868 Chen, C.T., Fernandez-Rhodes, L., Brzyski, R.G., Carlson, C.S., Chen, Z., Heiss, G., North, K.E., Woods, N.F.,
869 Rajkovic, A., Kooperberg, C., and Franceschini, N. (2012). Replication of loci influencing ages at
870 menarche and menopause in Hispanic women: the Women's Health Initiative SHARe Study. Hum Mol
871 Genet *21*, 1419-1432.
872 Circolo, A., Garnier, G., Fukuda, W., Wang, X., Hidvegi, T., Szalai, A.J., Briles, D.E., Volanakis, J.E., Wetsel,
873 R.A., and Colten, H.R. (1999). Genetic disruption of the murine complement C3 promoter region
874 generates deficient mice with extrahepatic expression of C3 mRNA. Immunopharmacology *42*, 135-149.
875 Clarkson, R.W., Wayland, M.T., Lee, J., Freeman, T., and Watson, C.J. (2004). Gene expression profiling of
876 mammary gland development reveals putative roles for death receptors and immune mediators in post-
877 lactational regression. Breast Cancer Res *6*, R92-109.
878 Day, F.R., Ruth, K.S., Thompson, D.J., Lunetta, K.L., Pervjakova, N., Chasman, D.I., Stolk, L., Finucane, H.K.,
879 Sulem, P., Bulik-Sullivan, B., Esko, T., Johnson, A.D., Elks, C.E., Franceschini, N., He, C., Altmaier, E., Brody,
880 J.A., Franke, L.L., Huffman, J.E., Keller, M.F.*, et al.* (2015). Large-scale genomic analyses link reproductive
881 aging to hypothalamic signaling, breast cancer susceptibility and BRCA1-mediated DNA repair. Nat
882 Genet *47*, 1294-1303.
883 Day, F.R., Thompson, D.J., Helgason, H., Chasman, D.I., Finucane, H., Sulem, P., Ruth, K.S., Whalen, S.,
884 Sarkar, A.K., Albrecht, E., Altmaier, E., Amini, M., Barbieri, C.M., Boutin, T., Campbell, A., Demerath, E.,
885 Giri, A., He, C., Hottenga, J.J., Karlsson, R.*, et al.* (2017). Genomic analyses identify hundreds of variants
886 associated with age at menarche and support a role for puberty timing in cancer risk. Nat Genet *49*, 834-
887 841.
888 DeFalco, T., Potter, S.J., Williams, A.V., Waller, B., Kan, M.J., and Capel, B. (2015). Macrophages
889 Contribute to the Spermatogonial Niche in the Adult Testis. Cell Rep *12*, 1107-1119.
890 Escudero-Esparza, A., Kalchishkova, N., Kurbasic, E., Jiang, W.G., and Blom, A.M. (2013). The novel
891 complement inhibitor human CUB and Sushi multiple domains 1 (CSMD1) protein promotes factor I-

892 mediated degradation of C4b and C3b and inhibits the membrane attack complex assembly. FASEB J *27*,
893 5083-5093.
894 Foldi, C.J., Eyles, D.W., McGrath, J.J., and Burne, T.H. (2011). The effects of breeding protocol in
895 C57BL/6J mice on adult offspring behaviour. PLoS One *6*, e18152.
896 Friddle, C.J., Abuin, A., Ramirez-Solis, R., Richter, L.J., Buxton, E.C., Edwards, J., Finch, R.A., Gupta, A.,
897 Hansen, G., Holt, K.H., Hu, Y., Huang, W., Jaing, C., Key, B.W., Jr., Kipp, P., Kohlhauff, B., Ma, Z.Q.,
898 Markesich, D., Newhouse, M., Perry, T.*, et al.* (2003). High-throughput mouse knockouts provide a
899 functional analysis of the genome. Cold Spring Harb Symp Quant Biol *68*, 311-315.
900 Gaytan, F., Morales, C., Bellido, C., Aguilar, E., and Sanchez-Criado, J.E. (1998). Ovarian follicle
901 macrophages: is follicular atresia in the immature rat a macrophage-mediated event? Biol Reprod *58*,
902 52-59.
903 Goldmann, J.M., Wong, W.S., Pinelli, M., Farrah, T., Bodian, D., Stittrich, A.B., Glusman, G., Vissers, L.E.,
904 Hoischen, A., Roach, J.C., Vockley, J.G., Veltman, J.A., Solomon, B.D., Gilissen, C., and Niederhuber, J.E.
905 (2016). Parent-of-origin-specific signatures of de novo mutations. Nat Genet *48*, 935-939.
906 Hays, J., Hunt, J.R., Hubbell, F.A., Anderson, G.L., Limacher, M., Allen, C., and Rossouw, J.E. (2003). The
907 Women's Health Initiative recruitment methods and results. Ann Epidemiol *13*, S18-77.
908 Hess, R.A., and Renato de Franca, L. (2008). Spermatogenesis and cycle of the seminiferous epithelium.
909 Adv Exp Med Biol *636*, 1-15.
910 Hoh Kam, J., Lenassi, E., Malik, T.H., Pickering, M.C., and Jeffery, G. (2013). Complement component C3
911 plays a critical role in protecting the aging retina in a murine model of age-related macular degeneration.
912 Am J Pathol *183*, 480-492.
913 Hotaling, J., and Carrell, D.T. (2014). Clinical genetic testing for male factor infertility: current
914 applications and future directions. Andrology *2*, 339-350.
915 Hsueh, A.J., Billig, H., and Tsafriri, A. (1994). Ovarian follicle atresia: a hormonally controlled apoptotic
916 process. Endocr Rev *15*, 707-724.
917 Huang, N., Wen, Y., Guo, X., Li, Z., Dai, J., Ni, B., Yu, J., Lin, Y., Zhou, W., Yao, B., Jiang, Y., Sha, J., Conrad,
918 D.F., and Hu, Z. (2015). A Screen for Genomic Disorders of Infertility Identifies MAST2 Duplications
919 Associated with Non-Obstructive Azoospermia in Humans. Biol Reprod.
920 Ingman, W.V., Wyckoff, J., Gouon-Evans, V., Condeelis, J., and Pollard, J.W. (2006). Macrophages
921 promote collagen fibrillogenesis around terminal end buds of the developing mammary gland. Dev Dyn
922 *235*, 3222-3229.
923 Kamal, M., Shaaban, A.M., Zhang, L., Walker, C., Gray, S., Thakker, N., Toomes, C., Speirs, V., and Bell,
924 S.M. (2010). Loss of CSMD1 expression is associated with high tumour grade and poor survival in
925 invasive ductal breast carcinoma. Breast Cancer Res Treat *121*, 555-563.
926 Kato, S., Shiratsuchi, A., Nagaosa, K., and Nakanishi, Y. (2005). Phosphatidylserine- and integrin-
927 mediated phagocytosis of apoptotic luteal cells by macrophages of the rat. Dev Growth Differ *47*, 153-
928 161.
929 Kim, D., Pertea, G., Trapnell, C., Pimentel, H., Kelley, R., and Salzberg, S.L. (2013). TopHat2: accurate
930 alignment of transcriptomes in the presence of insertions, deletions and gene fusions. Genome Biol *14*,
931 R36.
932 Kircher, M., Witten, D.M., Jain, P., O'Roak, B.J., Cooper, G.M., and Shendure, J. (2014). A general
933 framework for estimating the relative pathogenicity of human genetic variants. Nat Genet *46*, 310-315.
934 Korn, J.M., Kuruvilla, F.G., McCarroll, S.A., Wysoker, A., Nemesh, J., Cawley, S., Hubbell, E., Veitch, J.,
935 Collins, P.J., Darvishi, K., Lee, C., Nizzari, M.M., Gabriel, S.B., Purcell, S., Daly, M.J., and Altshuler, D.
936 (2008). Integrated genotype calling and association analysis of SNPs, common copy number
937 polymorphisms and rare CNVs. Nat Genet *40*, 1253-1260.

938 Kraus, D.M., Elliott, G.S., Chute, H., Horan, T., Pfenninger, K.H., Sanford, S.D., Foster, S., Scully, S.,
939 Welcher, A.A., and Holers, V.M. (2006). CSMD1 is a novel multiple domain complement-regulatory
940 protein highly expressed in the central nervous system and epithelial tissues. J Immunol *176*, 4419-4430.
941 Kumar, R.A., KaraMohamed, S., Sudi, J., Conrad, D.F., Brune, C., Badner, J.A., Gilliam, T.C., Nowak, N.J.,
942 Cook, E.H., Jr., Dobyns, W.B., and Christian, S.L. (2008). Recurrent 16p11.2 microdeletions in autism.
943 Hum Mol Genet *17*, 628-638.
944 Kurilo, L.F. (1981). Oogenesis in antenatal development in man. Hum Genet *57*, 86-92.
945 Laufer, J., Oren, R., Goldberg, I., Afek, A., Kopolovic, J., and Passwell, J.H. (1999). Local complement
946 genes expression in the mammary gland: effect of gestation and inflammation. Pediatr Res *46*, 608-612.
947 Lee, S., Emond, M.J., Bamshad, M.J., Barnes, K.C., Rieder, M.J., Nickerson, D.A., Team, N.G.E.S.P.-E.L.P.,
948 Christiani, D.C., Wurfel, M.M., and Lin, X. (2012). Optimal unified approach for rare-variant association
949 testing with application to small-sample case-control whole-exome sequencing studies. Am J Hum Genet
950 *91*, 224-237.
951 Lesher, A.M., Zhou, L., Kimura, Y., Sato, S., Gullipalli, D., Herbert, A.P., Barlow, P.N., Eberhardt, H.U.,
952 Skerka, C., Zipfel, P.F., Hamano, T., Miwa, T., Tung, K.S., and Song, W.C. (2013). Combination of factor H
953 mutation and properdin deficiency causes severe C3 glomerulonephritis. J Am Soc Nephrol *24*, 53-65.
954 Li, J., Witten, D.M., Johnstone, I.M., and Tibshirani, R. (2012). Normalization, testing, and false discovery
955 rate estimation for RNA-sequencing data. Biostatistics *13*, 523-538.
956 Li, R., and Albertini, D.F. (2013). The road to maturation: somatic cell interaction and self-organization of
957 the mammalian oocyte. Nat Rev Mol Cell Biol *14*, 141-152.
958 Li, S., Zhou, W., Doglio, L., and Goldberg, E. (1998). Transgenic mice demonstrate a testis-specific
959 promoter for lactate dehydrogenase, LDHC. J Biol Chem *273*, 31191-31194.
960 Lie, P.P., Mruk, D.D., Lee, W.M., and Cheng, C.Y. (2010). Cytoskeletal dynamics and spermatogenesis.
961 Philos Trans R Soc Lond B Biol Sci *365*, 1581-1592.
962 Lima, A.C., Jung, M., Rusch, J., Usmani, A., Lopes, A., and Conrad, D.F. (2016). Multispecies Purification of
963 Testicular Germ Cells. Biol Reprod *95*, 85.
964 Lipkin, S.M., Moens, P.B., Wang, V., Lenzi, M., Shanmugarajah, D., Gilgeous, A., Thomas, J., Cheng, J.,
965 Touchman, J.W., Green, E.D., Schwartzberg, P., Collins, F.S., and Cohen, P.E. (2002). Meiotic arrest and
966 aneuploidy in MLH3-deficient mice. Nat Genet *31*, 385-390.
967 Liszewski, M.K., Farries, T.C., Lublin, D.M., Rooney, I.A., and Atkinson, J.P. (1996). Control of the
968 complement system. Adv Immunol *61*, 201-283.
969 Lopes, A.M., Aston, K.I., Thompson, E., Carvalho, F., Goncalves, J., Huang, N., Matthiesen, R., Noordam,
970 M.J., Quintela, I., Ramu, A., Seabra, C., Wilfert, A.B., Dai, J., Downie, J.M., Fernandes, S., Guo, X., Sha, J.,
971 Amorim, A., Barros, A., Carracedo, A.*, et al.* (2013). Human spermatogenic failure purges deleterious
972 mutation load from the autosomes and both sex chromosomes, including the gene DMRT1. PLoS Genet
973 *9*, e1003349.
974 Luborsky, J.L., Meyer, P., Sowers, M.F., Gold, E.B., and Santoro, N. (2003). Premature menopause in a
975 multi-ethnic population study of the menopause transition. Hum Reprod *18*, 199-206.
976 Matzuk, M.M., and Lamb, D.J. (2008). The biology of infertility: research advances and clinical challenges.
977 Nat Med *14*, 1197-1213.
978 Murray, S.A., Morgan, J.L., Kane, C., Sharma, Y., Heffner, C.S., Lake, J., and Donahue, L.R. (2010). Mouse
979 gestation length is genetically determined. PLoS One *5*, e12418.
980 Myers, M., Britt, K.L., Wreford, N.G., Ebling, F.J., and Kerr, J.B. (2004). Methods for quantifying follicular
981 numbers within the mouse ovary. Reproduction *127*, 569-580.
982 Nelson, L.M. (2009). Clinical practice. Primary ovarian insufficiency. N Engl J Med *360*, 606-614.
983 Ni, B., Lin, Y., Sun, L., Zhu, M., Li, Z., Wang, H., Yu, J., Guo, X., Zuo, X., Dong, J., Xia, Y., Wen, Y., Wu, H., Li,
984 H., Zhu, Y., Ping, P., Chen, X., Dai, J., Jiang, Y., Xu, P.*, et al.* (2015). Low-frequency germline variants

985 across 6p22.2-6p21.33 are associated with non-obstructive azoospermia in Han Chinese men. Hum Mol
986 Genet *24*, 5628-5636.
987 Nusbaum, C., Mikkelsen, T.S., Zody, M.C., Asakawa, S., Taudien, S., Garber, M., Kodira, C.D., Schueler,
988 M.G., Shimizu, A., Whittaker, C.A., Chang, J.L., Cuomo, C.A., Dewar, K., FitzGerald, M.G., Yang, X., Allen,
989 N.R., Anderson, S., Asakawa, T., Blechschmidt, K., Bloom, T.*, et al.* (2006). DNA sequence and analysis of
990 human chromosome 8. Nature *439*, 331-335.
991 O'Flynn O'Brien, K.L., Varghese, A.C., and Agarwal, A. (2010). The genetic causes of male factor infertility:
992 a review. Fertil Steril *93*, 1-12.
993 Ogundele, M.O. (1999). Anti-complement activities of human breast-milk. Inflamm Res *48*, 437-445.
994 Perricone, R., Pasetto, N., De Carolis, C., Vaquero, E., Piccione, E., Baschieri, L., and Fontana, L. (1992).
995 Functionally active complement is present in human ovarian follicular fluid and can be activated by
996 seminal plasma. Clin Exp Immunol *89*, 154-157.
997 Perry, J.R., Day, F., Elks, C.E., Sulem, P., Thompson, D.J., Ferreira, T., He, C., Chasman, D.I., Esko, T.,
998 Thorleifsson, G., Albrecht, E., Ang, W.Q., Corre, T., Cousminer, D.L., Feenstra, B., Franceschini, N., Ganna,
999 A., Johnson, A.D., Kjellqvist, S., Lunetta, K.L.*, et al.* (2014). Parent-of-origin-specific allelic associations
1000 among 106 genomic loci for age at menarche. Nature *514*, 92-97.
1001 Pollard, J.W. (2009). Trophic macrophages in development and disease. Nat Rev Immunol *9*, 259-270.
1002 Pompon, J., and Levashina, E.A. (2015). A New Role of the Mosquito Complement-like Cascade in Male
1003 Fertility in Anopheles gambiae. PLoS Biol *13*, e1002255.
1004 Riley-Vargas, R.C., Lanzendorf, S., and Atkinson, J.P. (2005). Targeted and restricted complement
1005 activation on acrosome-reacted spermatozoa. J Clin Invest *115*, 1241-1249.
1006 Schafer, D.P., Lehrman, E.K., Kautzman, A.G., Koyama, R., Mardinly, A.R., Yamasaki, R., Ransohoff, R.M.,
1007 Greenberg, M.E., Barres, B.A., and Stevens, B. (2012). Microglia sculpt postnatal neural circuits in an
1008 activity and complement-dependent manner. Neuron *74*, 691-705.
1009 Schizophrenia Psychiatric Genome-Wide Association Study, C. (2011). Genome-wide association study
1010 identifies five new schizophrenia loci. Nat Genet *43*, 969-976.
1011 Schizophrenia Working Group of the Psychiatric Genomics, C. (2014). Biological insights from 108
1012 schizophrenia-associated genetic loci. Nature *511*, 421-427.
1013 Sekar, A., Bialas, A.R., de Rivera, H., Davis, A., Hammond, T.R., Kamitaki, N., Tooley, K., Presumey, J.,
1014 Baum, M., Van Doren, V., Genovese, G., Rose, S.A., Handsaker, R.E., Schizophrenia Working Group of the
1015 Psychiatric Genomics, C., Daly, M.J., Carroll, M.C., Stevens, B., and McCarroll, S.A. (2016). Schizophrenia
1016 risk from complex variation of complement component 4. Nature *530*, 177-183.
1017 Soumillon, M., Necsulea, A., Weier, M., Brawand, D., Zhang, X., Gu, H., Barthes, P., Kokkinaki, M., Nef, S.,
1018 Gnirke, A., Dym, M., de Massy, B., Mikkelsen, T.S., and Kaessmann, H. (2013). Cellular source and
1019 mechanisms of high transcriptome complexity in the mammalian testis. Cell Rep *3*, 2179-2190.
1020 Steen, V.M., Nepal, C., Ersland, K.M., Holdhus, R., Naevdal, M., Ratvik, S.M., Skrede, S., and Havik, B.
1021 (2013). Neuropsychological deficits in mice depleted of the schizophrenia susceptibility gene CSMD1.
1022 PLoS One *8*, e79501.
1023 Stegle, O., Parts, L., Piipari, M., Winn, J., and Durbin, R. (2012). Using probabilistic estimation of
1024 expression residuals (PEER) to obtain increased power and interpretability of gene expression analyses.
1025 Nat Protoc *7*, 500-507.
1026 Sternlicht, M.D. (2006). Key stages in mammary gland development: the cues that regulate ductal
1027 branching morphogenesis. Breast Cancer Res *8*, 201.
1028 Stolk, L., Perry, J.R., Chasman, D.I., He, C., Mangino, M., Sulem, P., Barbalic, M., Broer, L., Byrne, E.M.,
1029 Ernst, F., Esko, T., Franceschini, N., Gudbjartsson, D.F., Hottenga, J.J., Kraft, P., McArdle, P.F., Porcu, E.,
1030 Shin, S.Y., Smith, A.V., van Wingerden, S.*, et al.* (2012). Meta-analyses identify 13 loci associated with
1031 age at menopause and highlight DNA repair and immune pathways. Nat Genet *44*, 260-268.

1032 Sudlow, C., Gallacher, J., Allen, N., Beral, V., Burton, P., Danesh, J., Downey, P., Elliott, P., Green, J.,
1033 Landray, M., Liu, B., Matthews, P., Ong, G., Pell, J., Silman, A., Young, A., Sprosen, T., Peakman, T., and
1034 Collins, R. (2015). UK biobank: an open access resource for identifying the causes of a wide range of
1035 complex diseases of middle and old age. PLoS Med *12*, e1001779.
1036 Tingen, C.M., Kiesewetter, S.E., Jozefik, J., Thomas, C., Tagler, D., Shea, L., and Woodruff, T.K. (2011). A
1037 macrophage and theca cell-enriched stromal cell population influences growth and survival of immature
1038 murine follicles in vitro. Reproduction *141*, 809-820.
1039 Tryka, K.A., Hao, L., Sturcke, A., Jin, Y., Wang, Z.Y., Ziyabari, L., Lee, M., Popova, N., Sharopova, N.,
1040 Kimura, M., and Feolo, M. (2014). NCBI's Database of Genotypes and Phenotypes: dbGaP. Nucleic Acids
1041 Res *42*, D975-979.
1042 Wallace, W.H., and Kelsey, T.W. (2010). Human ovarian reserve from conception to the menopause.
1043 PLoS One *5*, e8772.
1044 Wang, K., Li, M., Hadley, D., Liu, R., Glessner, J., Grant, S.F., Hakonarson, H., and Bucan, M. (2007).
1045 PennCNV: an integrated hidden Markov model designed for high-resolution copy number variation
1046 detection in whole-genome SNP genotyping data. Genome Res *17*, 1665-1674.
1047 Wei, P.C., Chang, A.N., Kao, J., Du, Z., Meyers, R.M., Alt, F.W., and Schwer, B. (2016). Long Neural Genes
1048 Harbor Recurrent DNA Break Clusters in Neural Stem/Progenitor Cells. Cell *164*, 644-655.
1049 Weiss, L.A., Shen, Y., Korn, J.M., Arking, D.E., Miller, D.T., Fossdal, R., Saemundsen, E., Stefansson, H.,
1050 Ferreira, M.A., Green, T., Platt, O.S., Ruderfer, D.M., Walsh, C.A., Altshuler, D., Chakravarti, A., Tanzi, R.E.,
1051 Stefansson, K., Santangelo, S.L., Gusella, J.F., Sklar, P*., et al.* (2008). Association between microdeletion
1052 and microduplication at 16p11.2 and autism. N Engl J Med *358*, 667-675.
1053 White, J.K., Gerdin, A.K., Karp, N.A., Ryder, E., Buljan, M., Bussell, J.N., Salisbury, J., Clare, S., Ingham, N.J.,
1054 Podrini, C., Houghton, R., Estabel, J., Bottomley, J.R., Melvin, D.G., Sunter, D., Adams, N.C., Sanger
1055 Institute Mouse Genetics, P., Tannahill, D., Logan, D.W., Macarthur, D.G*., et al.* (2013). Genome-wide
1056 generation and systematic phenotyping of knockout mice reveals new roles for many genes. Cell *154*,
1057 452-464.
1058 Willott, G.M. (1982). Frequency of azoospermia. Forensic Sci Int *20*, 9-10.
1059 Wilson, T.E., Arlt, M.F., Park, S.H., Rajendran, S., Paulsen, M., Ljungman, M., and Glover, T.W. (2015).
1060 Large transcription units unify copy number variants and common fragile sites arising under replication
1061 stress. Genome Res *25*, 189-200.
1062 Yatsenko, A.N., Georgiadis, A.P., Ropke, A., Berman, A.J., Jaffe, T., Olszewska, M., Westernstroer, B.,
1063 Sanfilippo, J., Kurpisz, M., Rajkovic, A., Yatsenko, S.A., Kliesch, S., Schlatt, S., and Tuttelmann, F. (2015).
1064 X-linked TEX11 mutations, meiotic arrest, and azoospermia in infertile men. N Engl J Med *372*, 2097-
1065 2107.
1066 Zhao, H., Xu, J., Zhang, H., Sun, J., Sun, Y., Wang, Z., Liu, J., Ding, Q., Lu, S., Shi, R., You, L., Qin, Y., Zhao, X.,
1067 Lin, X., Li, X., Feng, J., Wang, L., Trent, J.M., Xu, C., Gao, Y*., et al.* (2012). A genome-wide association
1068 study reveals that variants within the HLA region are associated with risk for nonobstructive
1069 azoospermia. Am J Hum Genet *90*, 900-906.
1070 Zudaire, E., Gambardella, L., Kurcz, C., and Vermeren, S. (2011). A computational tool for quantitative
1071 analysis of vascular networks. PLoS One *6*, e27385.

1072

1073

1074

1075 **Figure Legends**

1076

1077 **Figure 1. The landscape of rare mutations across *CSMD1* in humans.**

1078 **(A)** Rare CNVs associated with gonadal function. We performed a gene-based genomewide

1079 association study to identify rare CNVs associated with female gonadal dysfunction (stage I) and

1080 attempted replication in males (stage II). All genes with nominal associations p-values < 0.05 in

1081 stage I, and the analogous values for stage II are listed; a value of "N/A" indicates that no CNVs

1082 were observed at the locus. Of note, biallelic knockout of *Mcph1* was reported to cause infertility

1083 in male and female mice (White et al., 2013).

1084 **(B)** Location of 37 rare (MAF < 0.01) SNVs overlapping *CSMD1* among 1,526 exome-

1085 sequenced females, and large, rare CNV regions overlapping *CSMD1* among 14,074 females and

1086 males (836 cases and 13,238 controls). CNV regions found in males are outlined by a dashed

1087 box. Additional tracks: "UKBB", the location of all rare intron 1-3 deletions observed in the UK

1088 Biobank POI cohort – for clarity only the deletions observed in cases are shown; "menarche

1089 GWAS SNPs", the location of three statistically independent lead SNPs from a large-scale

1090 GWAS of age at menarche are depicted as arrows along the bottom of the figure: rs2688326, rs

1091 2724961, and rs4875424 (Day et al., 2017).

1092 **(C)** Stacked barplot depicting frequency of rare (MAF < 1%) CNVs overlapping introns 1-3 of

1093 *CSMD1* among 2,702 cases of male or female gonadal dysfunction versus 72,194 controls. Rare

1094 deletions over *CSMD1* segregate significantly with cases (OR = 4.09; meta-analysis p = 4.8 x

1095 10^{-5}).

1096 **(D)** Boxplot depicting the effect size of rare *CSMD1* SNVs found in females, stratified by protein
1097 domain (CUB, Sushi, or neither). SNVs occurring in the CUB domains are significantly
1098 associated with an earlier onset of menopause when compared to SNVs in the Sushi domains
1099 (β_{CUB} = -0.86, 95% CI [-1.56, -0.151]; β_{SUSHI} = 0.046, 95% CI [-0.255, 0.377]; P = 0.043;
1100 Wilcoxon rank-sum test).
1101 **(E)** *De novo* mutation (DNM) frequency across chromosome 8. DNMs were called from whole
1102 genome sequence data for 709 parent-offspring trios. DNMs were compiled across 100 kb
1103 windows across chromosome 8 and a smoothing spline function was applied to the data (blue
1104 line). We used a mutation-rate prediction model to estimate context-dependent mutation rates for
1105 all bases on chromosome 8, averaged these across fixed 100 kb windows (grey line). Solid
1106 horizontal lines represent the mean value across chromosome 8, dotted horizontal lines represent
1107 1 standard deviation about the mean, and the pink shaded region represents the interval
1108 encompassing *CSMD1*.$\hat{\mu}$, the estimated germline mutation rate per base-pair, per generation.
1109

1110 **Figure 2. *Csmd1* is expressed in the male and female gonads.**
1111 **(A)** Protein model of CSMD1 in human and mouse. CUB and Sushi domains, as well as the
1112 transmembrane and cytosolic domains are depicted along the protein model (97.1% of the
1113 CSMD1 protein is extracellular).
1114 **(B)** RNA expression of mouse *Csmd1* in sexually immature whole testes (20 days), sexually
1115 mature whole testes (40 days), and whole ovary. RNA-seq of FACS-purified germ cell
1116 populations show *Csmd1* expression changes during spermatogenesis. *Csmd1* RNA is maximally
1117 expressed at the spermatid stage of development.

1118 **(C)** Immunofluorescence (IF) visualization of CSMD1 (red) in testis seminiferous tubule cross
1119 sections (x-y axis). CSMD1 protein is broadly expressed in germ cells across all stages of
1120 spermatogenesis. MVH is a primordial germ cell marker whose expression peaks early, then
1121 steadily decreases during spermatogenesis/oogenesis. CSMD1 is maximally expressed on
1122 elongating spermatids during the spermiation process with somatic Sertoli cells (white
1123 arrowheads).
1124 **(D)** Whole mount testis tubule preparation (z axis). F480-positive macrophages (green) with
1125 characteristic ramified processes occupy the interstitial space. CSMD1 (red) is expressed in a
1126 hatched pattern which may correspond to the actin cytoskeleton of peritubular myoid cells and
1127 Sertoli cells. Four Sertoli cells surrounding a macrophage outlined by dotted lines.
1128 **(E)** IF of CSMD1 in developing oocytes (marked by MVH) and surrounding somatic cells. MVH
1129 expression decreases whereas CSMD1 expression increases with follicular development.
1130 CSMD1 is seen coating the oocytes at all follicle stages, occasionally staining weakly in
1131 granulosa cells, and staining more strongly on theca cells. Follicles named in each box are
1132 marked with white arrows when necessary. Theca cells are indicated by stars.
1133 **(F)** CSMD1 is maximally expressed at the oocyte surface and extends into the transzonal
1134 projections (white arrowheads), which physically connect the germ cell to the surrounding
1135 somatic granulosa cells. During ovulation the follicle releases the oocyte and regresses to form
1136 the corpus luteum (dashed lines). CSMD1 and MVH signal is absent.
1137
1138 **Figure 3. *Csmd1* knockout testes show profound and heterogeneous morphologic**
1139 **degeneration.**
1140 **(A)** Seminferous tubule H&E histology of *Csmd1* wildtype and knockout littermates at 34 days

1141 of age. The majority of knockout tubules can be classified as "Sertoli cell-only" and contain no
1142 germ cells. Severe inflammatory changes are also observed in the interstitial space.
1143 **(B)** Qualitative stages of progressive morphologic degeneration. Seminiferous tubules from
1144 *Csmd1* knockout males showing normal morphology; loss of spatiotemporal architecture, but
1145 retained germ cells in all stages of spermatogenesis ("Disorganized"); loss of early stage germ
1146 cells into the tubule lumen ("Sloughing"); loss of all germ cells except late-stage spermatids
1147 ("Missing waves"); and loss of all germ cells, leaving a signature of vacuolization ("Sertoli-
1148 only"). Early-stage ectopic germ cells can be observed in the downstream epididymis, likely
1149 from upstream sloughing tubules. *Csmd1* knockout males can show multiple stages of
1150 degeneration within an individual testis.
1151 **(C)** Quantification of the degeneration phenotype. Testis H & E sections from control (n=12) and
1152 *Csmd1* knockout (n=53) animals were visually classified into one of three degeneration
1153 phenotypes: "None", "Mild", or "Profound" (Methods). The stacked barplots depict the
1154 proportion of damaged tubules among wildtypes and knockouts, stratified by age group. Damage
1155 severity segregates significantly with genotype, even after accounting for age ($P = 7.69 \times 10^{-3}$;
1156 ANOVA).
1157 **(D)** TRA98/GCNA positive spermatogonial cells (green) are much less abundant, and stain less
1158 intensely, in tubules of *Csmd1* knockouts.
1159 **(E)** Raw biometry and fecundity measurements from Csmd1 mutant colony. The mean and
1160 standard deviation of each measurement is reported. All weights are in grams.
1161
1162

1163 **Figure 4. *Csmd1* knockout ovaries show reduced morphologic quality and reproductive**
1164 **performance.**

1165 **(A)** Ovarian histology in *Csmd1* wildtype versus knockout females. Knockout ovaries were
1166 consistently enriched for foam cell macrophages, compared to age-matched controls, as detected
1167 by Oil Red O staining. Adjacent sections from 265 day old wild type (left)_and 240 day old
1168 knockout (right). Asterices indicate a large ovarian cyst in the knockout animal. Cysts were
1169 occasionally noted in knockout but not control animals. **(B)** Left: ovary from 336 day-old
1170 knockout showing extensive involvement of foam cells occupying 40% of the tissue. Right: high
1171 magnification of ovary section from same animal; top shows multinucleated appearance of foam
1172 cells, bottom is oil red O staining of same site in adjacent section. **(C)** Knockout females (n=68)
1173 have significantly smaller ovaries than wildtype (n=27) when controlling for age ($p = 8.1 \times 10^{-3}$).
1174 A quadratic regression model (shown) provided better fit to the data than a linear model. The
1175 grey hashed line indicates approximate onset of puberty in females. (**D**) Knockout females show
1176 more atretic and fewer morphologically normal pre-ovulatory follicles in ovary sections ($p=3.5 \times$
1177 10^{-3}, Hotelling t-test). One section was evaluated per ovary. **(E)** Probability density plot
1178 depicting mating success over time, by female genotype. The probability density is periodic,
1179 corresponding to the female estrous cycle. Knockout females took significantly longer to achieve
1180 pregnancy ($\beta_{GT} = 10.4$, $P = 0.01$). All p-values reflect statistical models that account for
1181 confounders when appropriate such as age, body weight, and male factors.

1182

1183 **Figure 5. Knockout of *Csmd1* in mothers causes increased mortality in the offspring.**
1184 **(A)** Scatterplot of number of pups surviving the neonatal period of 10 days ("Offspring
1185 surviving") versus live births ("Offspring born") versus, by maternal genotype (*Csmd1* wildtype

1186 and heterozygote versus *Csmd1* knockout). Points that lie along the dashed line (slope = 1)
1187 represent litters with no neonatal deaths. Maternal *Csmd1* genotype is significantly associated
1188 with surviving litter size (% $mortality_{WT/het}$ = 10.5%; % $mortality_{KO}$ = 50.0%; P = 7.93 x 10^{-7};
1189 Poisson regression). Data points deviate slightly from whole numbers for ease of visualization.
1190 **(B)** IF shows CSMD1 expression in bifurcating mammary ducts and bulbous terminal end buds.
1191 CSMD1 is expressed on both luminal epithelial cells and myoepithelial cells of the ducts
1192 throughout the adult life cycle: expression is lowest at puberty and increases during pregnancy,
1193 with the highest intensity during involution. Scale bars, 50 μm. (**C**) Close-up of CSMD1 on the
1194 membrane of a myoepithelial cell surrounding an alveolus during lactation (dashed line; left).
1195 CSMD1 was also observed on the membrane of small stromal cells (right). Scale bars, 20 μm.
1196 **(D)** Whole-mount mammary glands of *Csmd1* wildtype and knockout littermates during mid-
1197 pregnancy (left) and post-weaning (right). Square bracketed numbers represent normalized
1198 percent density of the branching epithelial network. Scale bars, 5 mm. (**E**) Knockout ducts
1199 appear to have greatly reduced lateral branching compared to wildtype (white arrowheads). Scale
1200 bars, 0.5mm. (**F**) To confirm this, we used computational image analysis to make quantitative
1201 comparisons of the structure and size of mammary ducts from age-matched nongravid
1202 nulliparous adults (n = 5 knockouts and n = 6 wildtype). Of 5 measurements made, two showed
1203 significant differences: the density of branch points along the duct (JD, $p < 0.05$) and the density
1204 of end segment (EPD, $p < 0.01$). VPA = percentage of area occupied by ducts. JD = density of
1205 branchpoints per mm. TVL = sum of Euclidean distances between all adjacent branch points.
1206 AVL = average length of Euclidean distance between adjacent branch points. EPD = number of
1207 duct end points normalized by total vessel length.
1208

1209 **Figure 6. Complement C3 regulation in mouse testes and ovaries.**

1210 **(A)** RNA expression of mouse *C3* in sexually immature whole testes (20 days), sexually mature
1211 whole testes (40 days), and whole ovary. RNA-seq of FACS-purified germ cell populations show
1212 *C3* expression changes during spermatogenesis. *C3* is maximally expressed at the
1213 spermatogonium stage. *Csmd1* RNA-seq data from Figure 2 are rescaled and superimposed for
1214 ease of comparison. **(B)** Complement and macrophages are confined to the basal compartment in
1215 normal tubules. Whole mount tubule IF visualization of macrophage marker F480 along shows
1216 extensive macrophage abundance along the interstitium. Cross section of tubule shows C3
1217 expression in the interstitium, but not within the lumen. Cross section of downstream epididymis
1218 also shows continued exclusion of C3 from the lumen. Individual tubules are circumscribed by
1219 dashed lines. **(C)** Boxplots depicting F4/80 abundance and C3 deposition in FACS-sorted *Csmd1*
1220 wildtype versus knockout testes. Both F4/80 and C3 are increased in knockout testes, though
1221 only significant for C3 (2-tailed *t*-test; $P = 7.7 \times 10^{-4}$). **(D)** C3 and CSMD1 co-localize at the
1222 oocyte surface. In most follicles examined, C3 and CSMD1 co-localize at the oocyte plasma
1223 membrane with overlapping signal (top 2 panels). On rare occasion the two signals separate and
1224 C3 stains in a ring outside of CSMD1 (bottom 2 panels). **(E)** F4/80 IF of adjacent follicles
1225 shows positive signal in corpus luteum, but not in follicles, consistent with prior expectations. C3
1226 is expressed on the oocyte as well as in the follicular fluid of the developing antrum (asterisk).
1227 Atretic follicles at different stages of degeneration (white arrows) show varying levels of C3 and
1228 F4/80 expression. F4/80 can also be seen in a punctuated pattern along the stroma and thecal
1229 layers (white arrowheads), consistent with prior expectations. C3 signal is also seen in corpus
1230 luteum. Individual follicles are circumscribed by dashed lines. **(F)** C3 and CSMD1 also
1231 colocalize in mammaries. As early as puberty there is abundant C3 staining within mammary

1232 ducts with empty lumens (top panel) and ducts with cells in the lumen (middle panel). C3 is also

1233 present in vesicles of some CSMD1+ stromal cells (bottom panel).

1234

1235

FIGURE 1

A

		Nominal p-value	Corrected p-value	Replication p-value	
Chr	Gene	Female		Male	Female
1	*PRAMEF8*	0.0018	0.1944	N/A	N/A
1	*PRAMEF15*	0.0018	0.1944	N/A	N/A
1	*PRAMEF9*	0.0018	0.1944	N/A	N/A
1	*PRAMEF14*	0.0018	0.1944	N/A	N/A
8	*CSMD1*	0.0004	0.0148	0.0031	0.0004
8	*MCPH1*	0.0048	0.4169	N/A	N/A

B

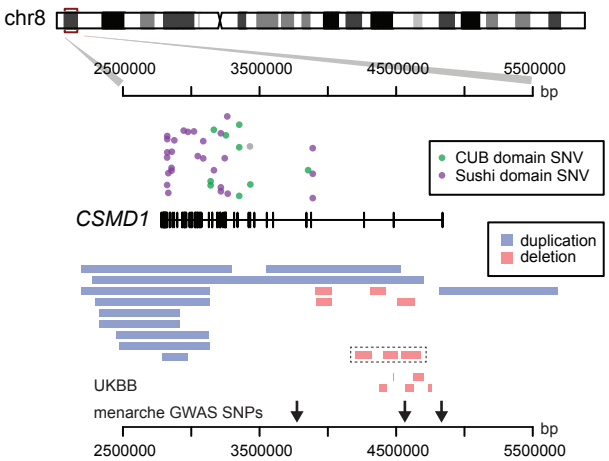

C

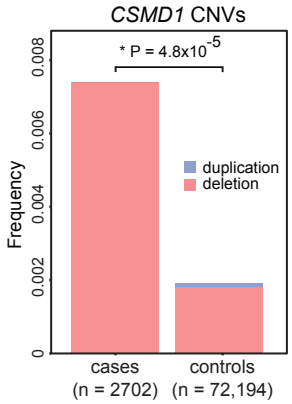

D

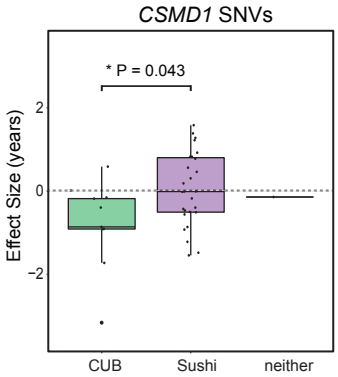

E

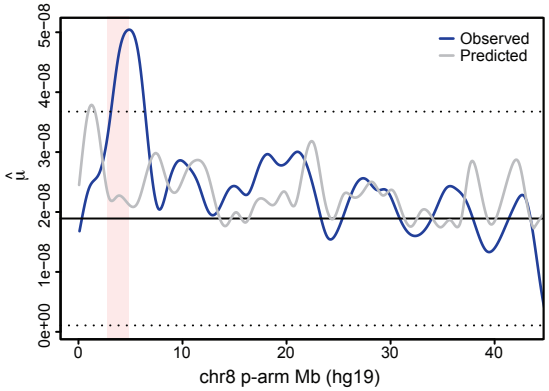

FIGURE 2

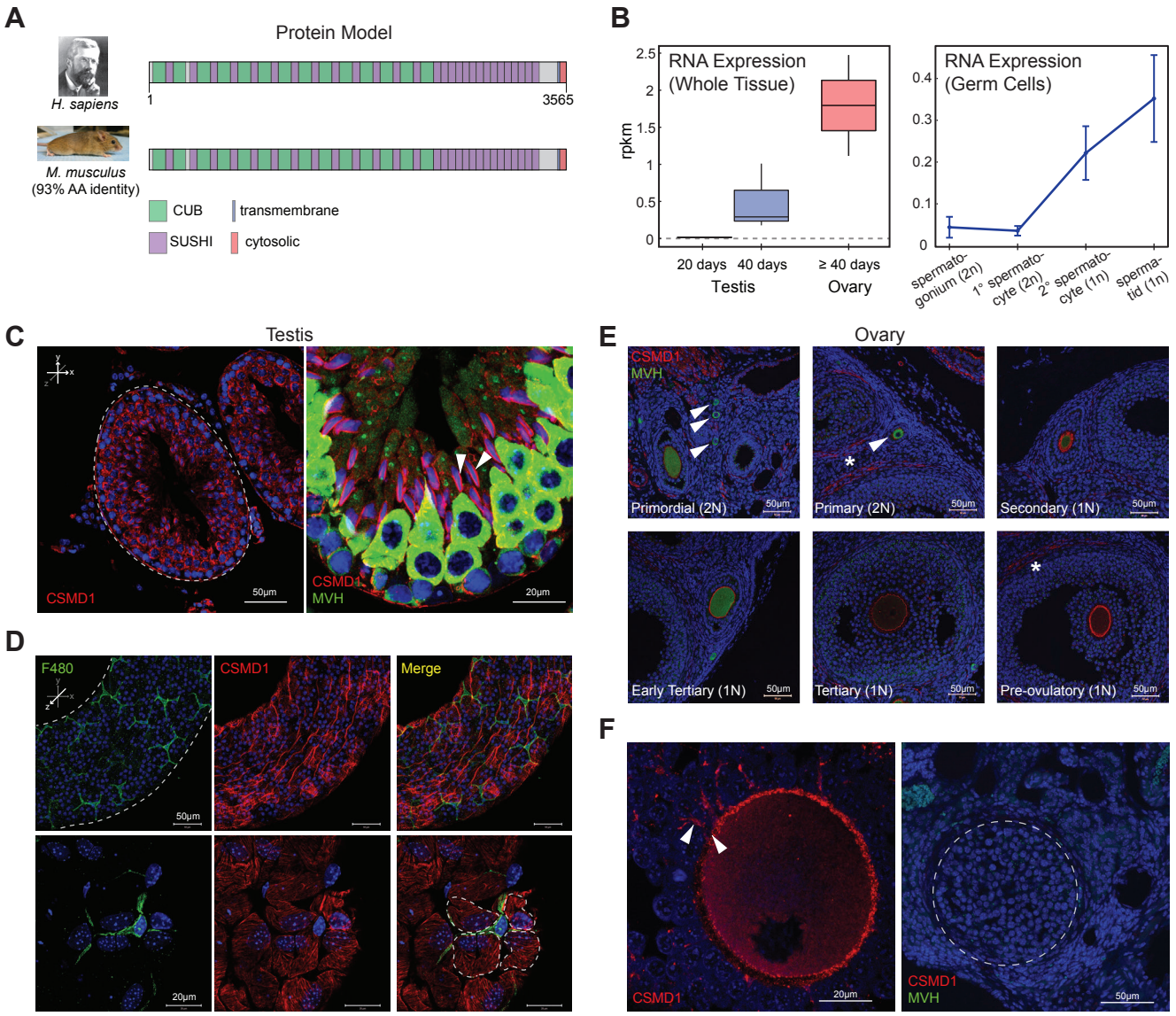
A
Protein Model
H. sapiens
1
3565
M. musculus
(93% AA identity)
CUB
transmembrane
SUSHI
cytosolic
B
RNA Expression
(Whole Tissue)
rpkm
2.5
2
1.5
1
0.5
0
20 days
40 days
≥ 40 days
Testis
Ovary
RNA Expression
(Germ Cells)
0.4
0.3
0.2
0.1
0
spermato-
gonium (2n)
1° spermato-
cyte (2n)
2° spermato-
cyte (1n)
sperma-
tid (1n)
C
Testis
CSMD1
50µm
CSMD1
MVH
20µm
D
F480
CSMD1
Merge
50µm
20µm
E
Ovary
CSMD1
MVH
Primordial (2N)
Primary (2N)
Secondary (1N)
Early Tertiary (1N)
Tertiary (1N)
Pre-ovulatory (1N)
50µm
F
CSMD1
20µm
CSMD1
MVH
50µm

FIGURE 3

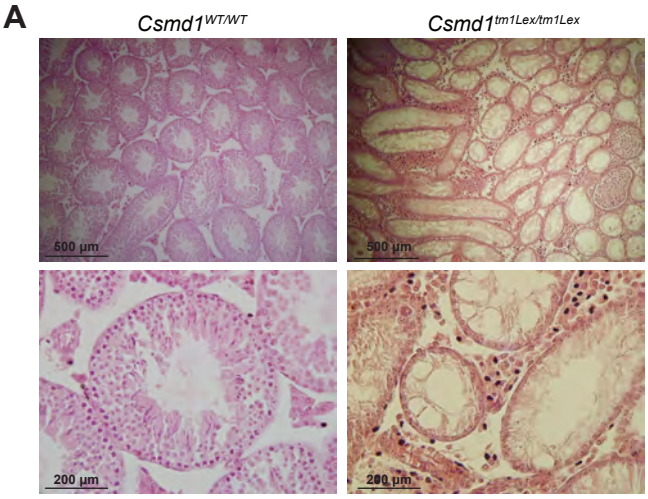

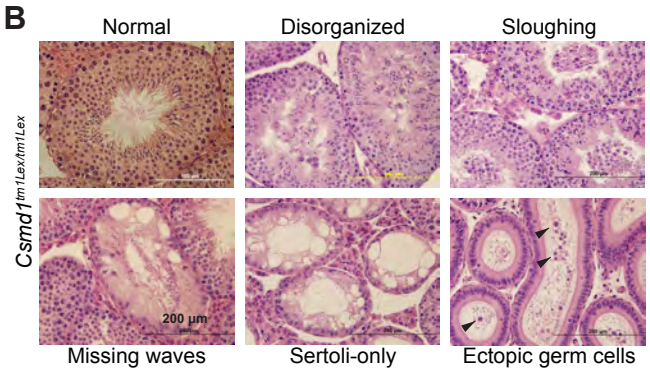

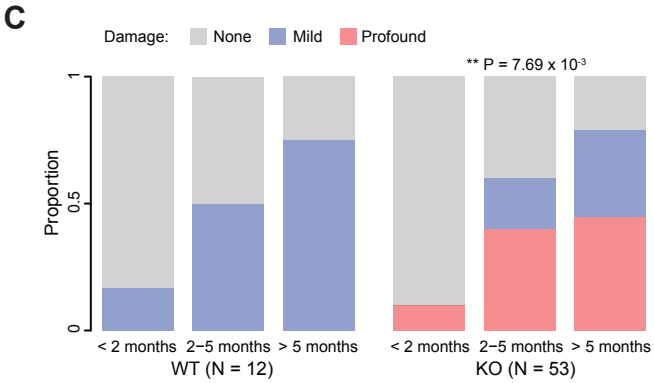

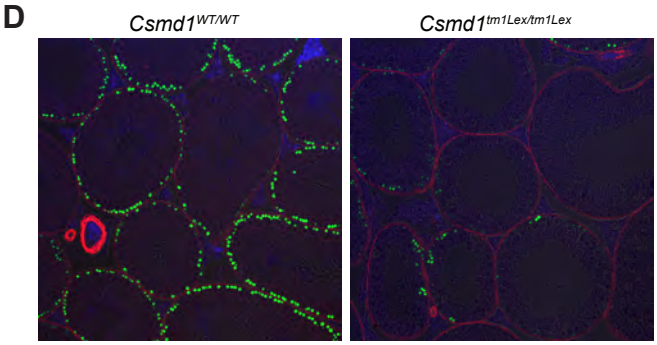

E

Male	WT	KO
Testes weight	0.29 [0.24 - 0.34]	0.27 [0.25 - 0.29]
Litter size	5.4 [3.4 - 7.4]	7.4 [6.6 - 8.2]
Female	**WT**	**KO**
Ovary weight	0.057 [0.024 - 0.090]	0.028 [0.017 - 0.039]
Mammary weight	0.48 [0.35 - 0.61]	0.37 [0.26 - 0.48]
Litter size	6.6 [5.4 - 7.8]	6.9 [5.7 - 8.1]

FIGURE 4

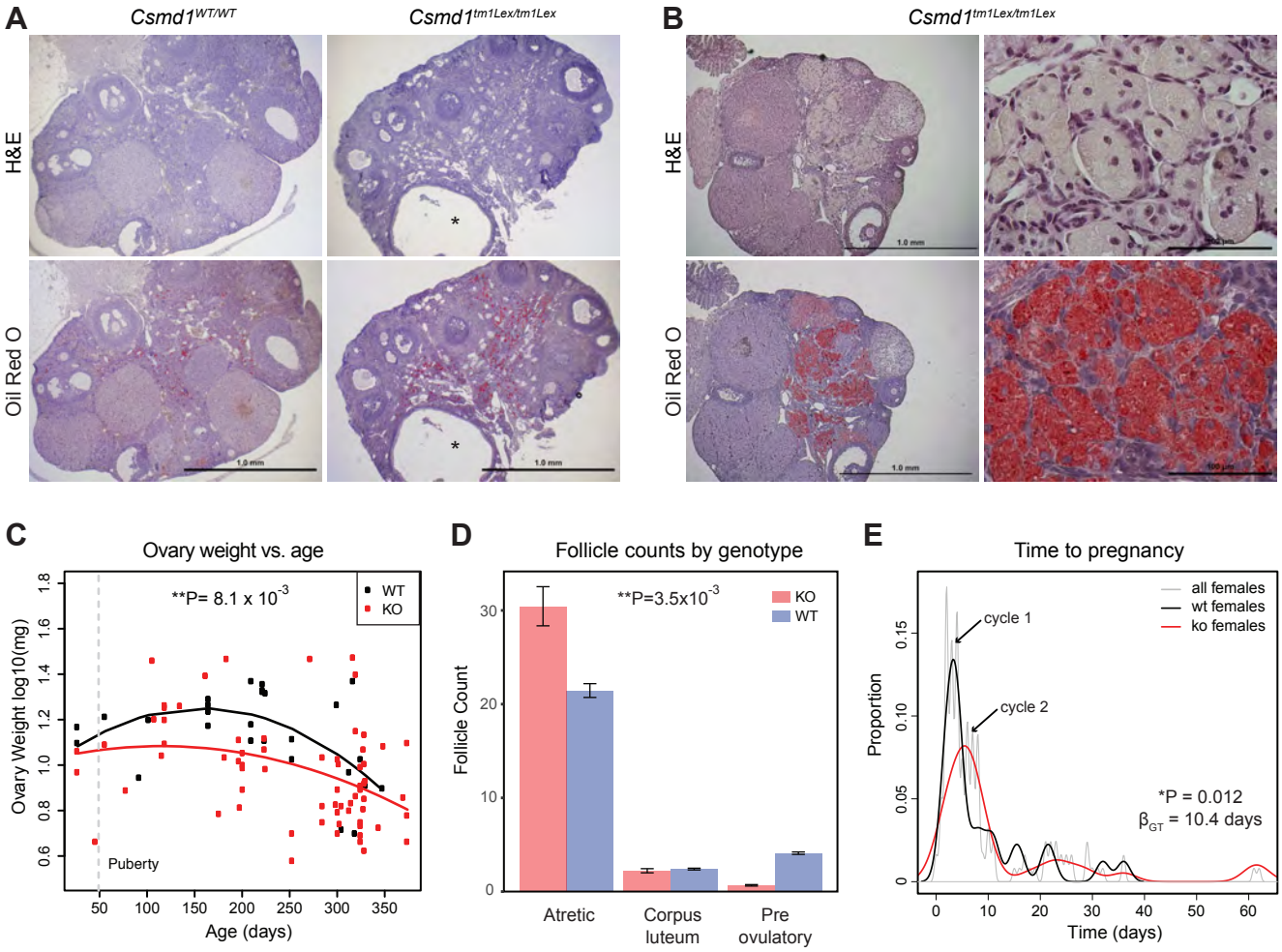
A
Csmd1WT/WT
Csmd1tm1Lex/tm1Lex
H&E
Oil Red O
B
Csmd1tm1Lex/tm1Lex
H&E
Oil Red O
C
Ovary weight vs. age
**P= 8.1 x 10-3
WT
KO
Ovary Weight log10(mg)
Puberty
Age (days)
D
Follicle counts by genotype
**P=3.5x10-3
KO
WT
Follicle Count
Atretic
Corpus luteum
Pre ovulatory
E
Time to pregnancy
all females
wt females
ko females
cycle 1
cycle 2
Proportion
*P = 0.012
βGT = 10.4 days
Time (days)

FIGURE 5

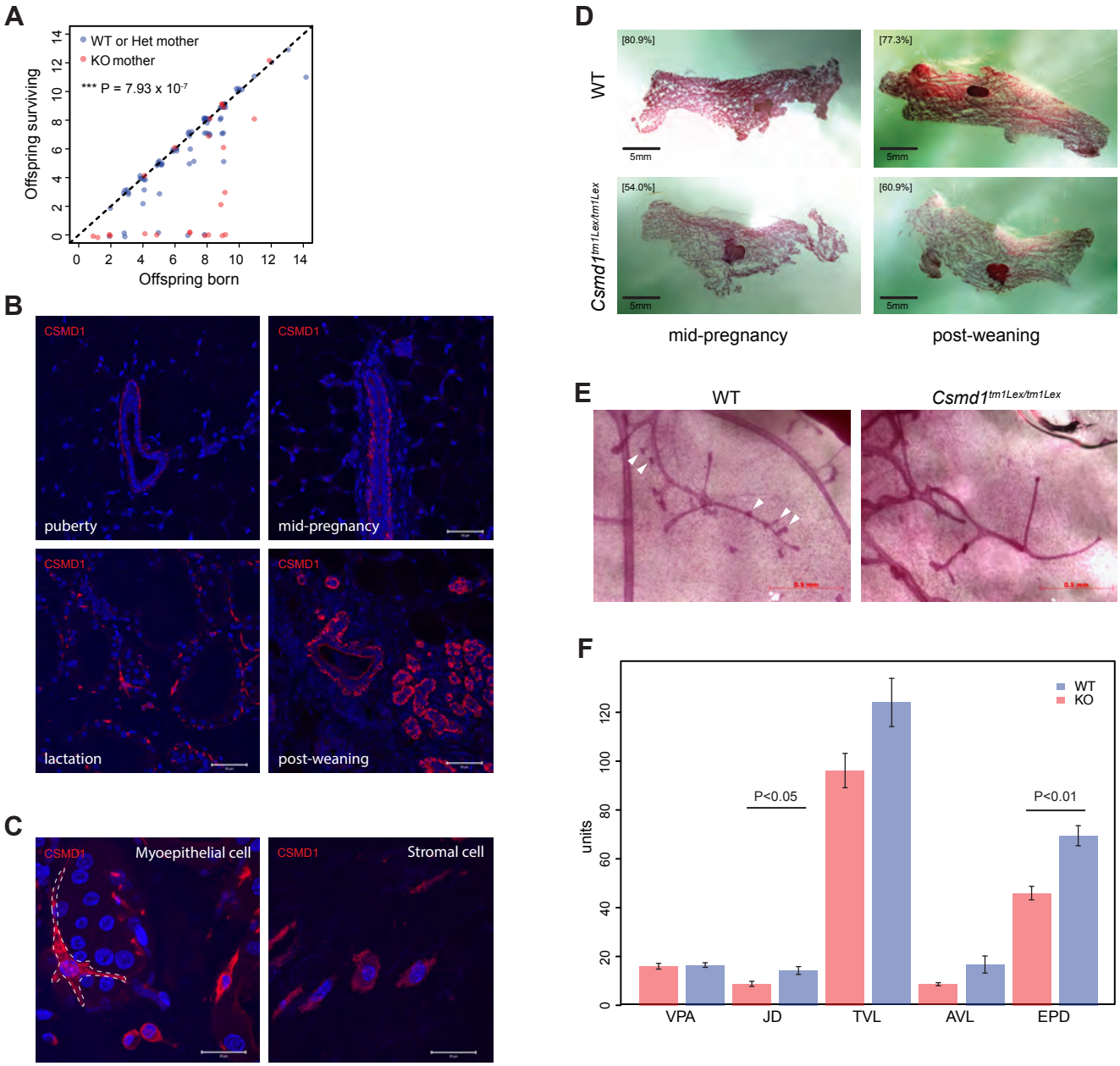
A
WT or Het mother
KO mother
*** P = 7.93 x 10-7
Offspring surviving
Offspring born
B
CSMD1
puberty
mid-pregnancy
lactation
post-weaning
C
Myoepithelial cell
Stromal cell
D
WT
Csmd1tm1Lex/tm1Lex
[80.9%]
[77.3%]
[54.0%]
[60.9%]
5mm
mid-pregnancy
post-weaning
E
WT
Csmd1tm1Lex/tm1Lex
F
WT
KO
units
P<0.05
P<0.01
VPA
JD
TVL
AVL
EPD

FIGURE 6

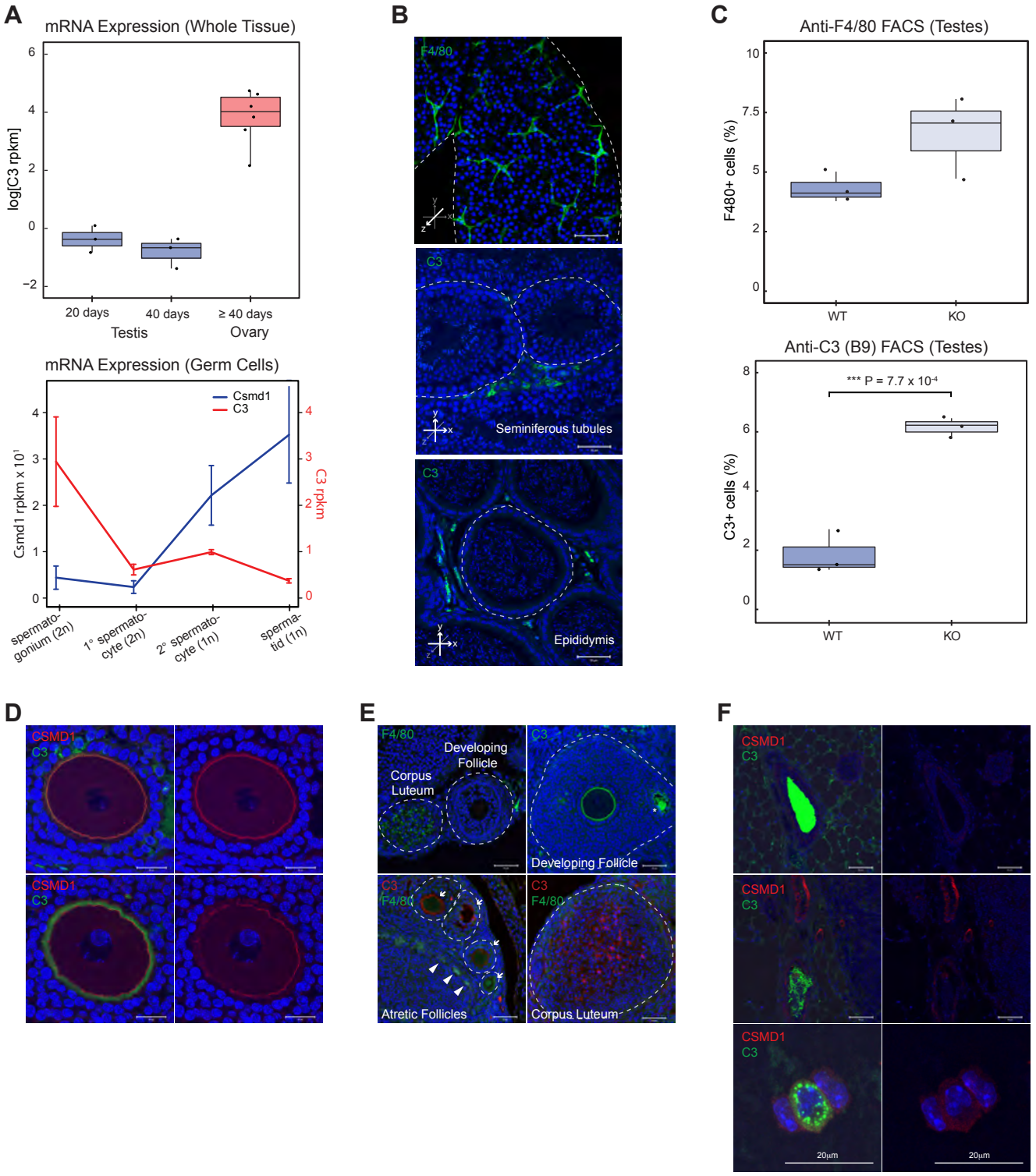
A
mRNA Expression (Whole Tissue)
log[C3 rpkm]
20 days
40 days
≥ 40 days
Testis
Ovary
mRNA Expression (Germ Cells)
Csmd1
C3
Csmd1 rpkm x 10¹
C3 rpkm
spermato-gonium (2n)
1° spermato-cyte (2n)
2° spermato-cyte (1n)
sperma-tid (1n)
B
F4/80
C3
Seminiferous tubules
C3
Epididymis
C
Anti-F4/80 FACS (Testes)
F480+ cells (%)
WT
KO
Anti-C3 (B9) FACS (Testes)
*** P = 7.7 x 10⁻⁴
C3+ cells (%)
WT
KO
D
CSMD1
C3
CSMD1
C3
E
F4/80
Developing Follicle
Corpus Luteum
C3
Developing Follicle
C3
F4/80
Atretic Follicles
C3
F4/80
Corpus Luteum
F
CSMD1
C3
CSMD1
C3
CSMD1
C3
20µm
20µm